Chapter 9

Ti-Al-N-Based Hard Coatings: Thermodynamical Background, CVD Deposition, and Properties. A Review

Florent Uny, Elisabeth Blanquet,
Frédéric Schuster and Frédéric Sanchette

Additional information is available at the end of the chapter

http://dx.doi.org/10.5772/intechopen.79747

Abstract

For several decades, the increasing productivity in many industrial domains has led to a significant and ever-increased interest to protective and hard coatings. In this context, titanium-aluminum nitrides were developed and are now widely used in a large range of applications, due to their high hardness, good thermal stability, and oxidation resistance. This chapter reviews the thermodynamical characteristics of the Ti-Al-N system by reporting the progress made in the description of the Ti-Al-N phase diagram and the main mechanical and chemical properties of $Ti_{1-x}Al_xN$-based coatings. As a metastable phase, the existence of the fcc-$Ti_{1-x}Al_xN$ depends on particular process parameters, allowing stabilizing this desirable solid solution. The influence of process parameters, with a particular interest for chemical vapor deposition (CVD) methods, on morphology and crystallographic structure is then described. The structure of $Ti_{1-x}Al_xN$ thin films depends also on the aluminum content as well as on the annealing temperature, due to the spinodal nature of the Ti-Al-N system. These changes of crystallographic structure can induce an improvement of the hardness, oxidation resistance, and wear behavior of these coatings. The main mechanical and chemical properties of physical vapor deposition (PVD) and CVD $Ti_{1-x}Al_xN$-based coatings are also described.

Keywords: TiAlN coatings, CVD, aluminum content dependence, mechanical properties, oxidation resistance

1. Introduction

Hard coatings started to be used at an industrial scale in the 1970s [1]. It was then titanium nitride (TiN) obtained by thermal CVD and deposited on tungsten carbide tools in order to

improve not only the lifetime of tools but also their behavior during machining. Physical vapor deposition technologies (PVD) were used in the mid-1980s for this type of application. "Vide et Traitement Holding" started this activity in France in 1984 with cathodic arc deposition technology, now widely used in this field. Titanium and chromium nitrides were the first materials on the market in the field of coatings for cutting tools or molds. The evolution of deposition reactors and research increasingly active on this issue has led to coatings with multilayer architecture. Thus, titanium carbonitride (TiCN), whose layered architecture is performed by modulating the introduction of reactive gases, led, in the early 1990s, to a significant change of machining performances under severe conditions. The evolution of both machining techniques, high-speed machining for example, and materials to be machined has led to new alloy developments such as $Ti_{1-x}Al_xN$ whose thermal stability and oxidation resistance, in particular, are better than that of TiN. $Ti_{1-x}Al_xN$ films are thus now industrially used in a wide range of applications, from hard and barrier coatings on cutting tools or molds [2] to electronic devices or optical coatings [3]. Since the late 1990s, new architectures have been introduced on the hard coatings market. Indeed, the nanostructuring of deposited materials has allowed an increase of hardness while keeping Young's modulus and internal residual stresses at relatively low values. These nanostructured coatings are essentially divided into two kinds: at first, the heterostructures (superlattice, nanolayered films), stacks of two materials with thicknesses of nanometer size, and secondly, the nanocomposites consisting of transition metal nitride crystallites of a nanoscale size in a matrix (nanocrystalline or amorphous) of a nonmetal covalent nitride [4]. This review chapter is focused mainly on the $Ti_{1-x}Al_xN$ material coatings. Thermodynamical basis and influence of the elaboration processes, especially the thermal CVD, on the structure of the coatings are discussed. The main properties (hardness, tribological properties, and oxidation resistance) of these coatings are finally described regarding their dependence on Al content and deposition temperature. The overall mechanisms related to these properties are also discussed. Information about other properties as thermal and electrical conductivity, hydrogen permeation, or thermal expansion, not presented here in details, should be found in [5–9].

2. Thermodynamical background

2.1. Phase thermodynamics basis

Phase stability (or metastability) is generally described using the change in Gibb's free energy G as a function of the concentration c. When $(\partial 2G)/\partial c2 \geq 0$, the system is thermodynamically stable (or metastable). If $(\partial 2G)/\partial c2 < 0$, the system is unstable and will decompose to form the stable phases. Actually, for a two-phase system (or more), the free energy of the system is described using a mixing term ΔGm. This free energy of mixing essentially defines the interactions between the atoms and so the ability of the system to form a solid solution or to segregate, i.e., to decompose into two distinct phases. This decomposition should be made by two different ways, depending on the value of the system's free energy. **Figure 1** shows the decomposition domains for a mixing of two elements A and B associated to the free energy

http://dx.doi.org/10.5772/intechopen.79747

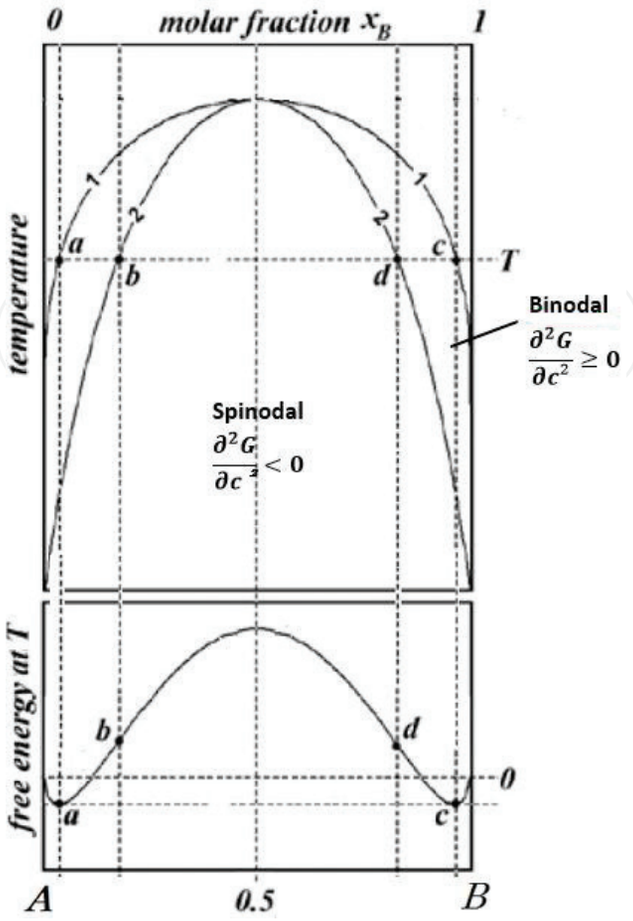

Figure 1. Schematic representation of a typical free energy curve at a temperature T with the associated decomposition domain. The two domains between the points "a-b" and "c-d" will show a nucleation-growth decomposition, while the "b-d" domain is related to the spinodal decomposition [10].

curve at the temperature T. The curves 1 and 2 delimit the domain of the binodal decomposition. Below the curve 2, the decomposition will be spinodal, and above the curve 1, the solid solution exists, regardless of the amount of the element B in the mixture. In the same way, on the G curve (G vs. chemical composition, **Figure 1**), a demixing domain is identified by the presence of a "hill" limited by two inflection points. Between these two points (points b and d on **Figure 1**), the demixing will be spinodal. Between the inflection points and the two minima of free energy (domains a-b and c-d on **Figure 1**), demixing will occur by nucleation-growth mechanism [10]. This G curve is associated to the demixing curves of the TiN-AlN system.

2.2. Ti-Al-N system

2.2.1. Stable diagram

Thermodynamic calculations have mainly aimed at stabilizing, experimentally, the ternary compounds as Ti_3AlN, $Ti_3Al_2N_2$, and particularly Ti_2AlN, because of its $M_{n+1}AX_n$ nature (where M is a transition metal, A is an A-group element, and X could be C or N and $1 < n < 3$) [11–14]. Many authors have reported phase diagrams with rather good agreement with

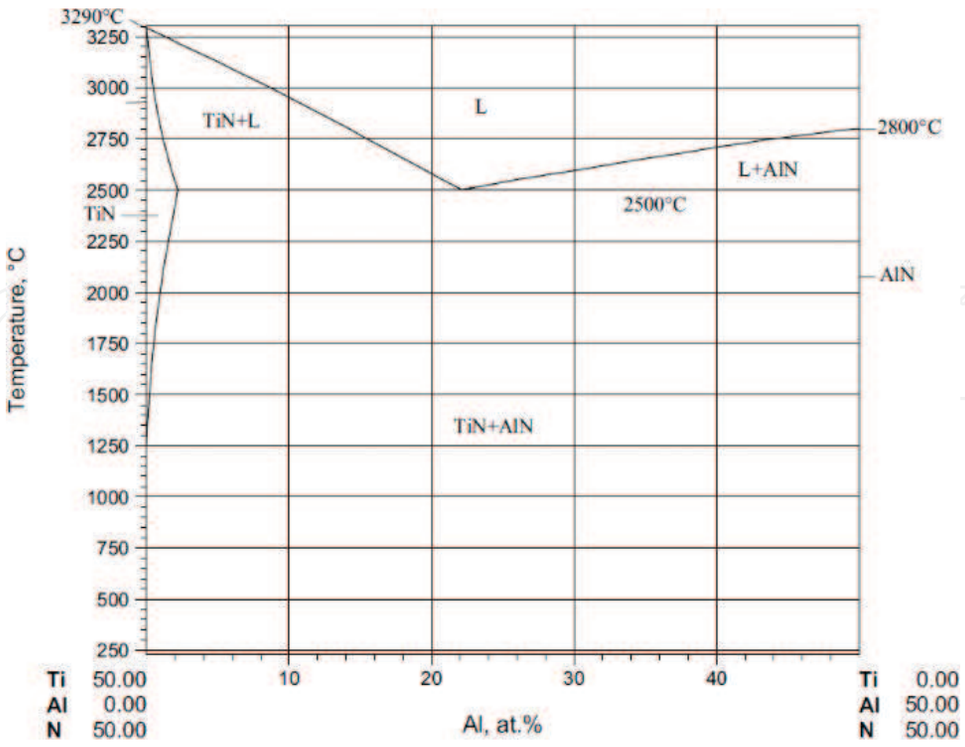

Figure 2. Pseudobinary TiN-AlN stable phase diagram [16].

experimental results. Especially, Chen and Sundman achieved a quite complete modeling up to 2500°C showing the evolution of the stability of these ternary compounds with temperature and establishing a thermodynamical database with a good reliability compared to experiments [15]. The pseudobinary diagram of the Ti-Al-N system is shown **Figure 2** [16]. It is clearly shown that mixing of AlN and TiN results in a biphased domain composed of the stable fcc-TiN and hcp-AlN on the entire range of composition. It is only from 1250°C that a little solubility of Al appears in the TiN structure.

2.2.2. Metastable diagram

As said previously, the thermodynamic aspects of the Ti-Al-N system do not predict the existence of the solid solution, the solubility of Al in TiN is very low. It implies that the experimentally observed $Ti_{1-x}Al_xN$ solid solution is a metastable phase, i.e., it is kinetically favorable to stabilize it rather than the stable phases. The metastable $Ti_{1-x}Al_xN$ phases can exist under two structures: an fcc-solid solution (also known as B1 structure), considered as the mixing of the stable fcc-TiN and the metastable fcc-AlN, and an hcp-solid solution (B4 structure), considered as the mixing of the metastable hcp-TiN and the stable hcp-AlN. The deposition kinetic then hinders the demixing and allows to stabilize these solid solutions [17, 18].

In order to better understand and discuss about the existence of the $Ti_{1-x}Al_xN$ solid solution, a lot of thermodynamical studies, and more recently ab initio calculations, have been realized for several decades. These calculations show that the shape of the ΔGm curve clearly leads to demixing. More, the system is typically spinodal [19], i.e., the $Ti_{1-x}Al_xN$

phase must spontaneously decompose into fcc-TiN and fcc-AlN. Then, with increasing time or temperature, fcc-AlN forms its hcp-AlN stable phase by germination and growth. This implies that fcc-TiN and fcc-AlN are thermodynamically immiscible (see **Figure 2**).

Considering that fcc-$Ti_{1-x}Al_xN$ solid solution is the result of the mixing of fcc-TiN and fcc-AlN, the thermodynamical modeling of this system is based on an equilibrium between these two phases with a total solubility. Anderbouhr et al. proposed thus a metastable ternary diagram of the Ti-Al-N system, showing the presence of the fcc-$Ti_{1-x}Al_xN$ phase on the whole range of aluminum content [20, 21]. Thermodynamic values for the lattice stability of fcc-AlN were based on experimental study led by Stolten et al. [17, 22]. However, experimental studies show that it is possible to deposit single-phased fcc-$Ti_{1-x}Al_xN$ with a maximum $x \approx 0.7$ for PVD processes as magnetron sputtering [23, 24] or cathodic arc [25, 26] and up to $x \approx 0.9$ for coatings deposited by thermal CVD [27] or PECVD [27–29] (with x defined as the Al/(Al + Ti) molar ratio). Above these values (x = 0.7 for PVD techniques and x = 0.9 for LPCVD), the deposition of a hexagonal phase occurs (hcp-$Ti_{1-x}Al_xN$ for PVD techniques and hcp-AlN for CVD processes). Thus, it seems to be difficult to correlate the modeling of the Ti-Al-N ternary phase diagram and these evolutions of structure with aluminum content.

Based on experimental results, a pseudobinary diagram (**Figure 3**) was proposed by Cremer et al. [30, 31] and confirmed by further experiments. This diagram is now widely accepted by many researchers. Although this diagram comes from experimental PVD data from films obtained by magnetron sputtering up to 700°C, other data for higher temperatures were extrapolated and are not in agreement with the current results, where deposition of an fcc-$Ti_{1-x}Al_xN$ single-phased film was obtained by LPCVD and PECVD up to x = 0.9 [27, 28].

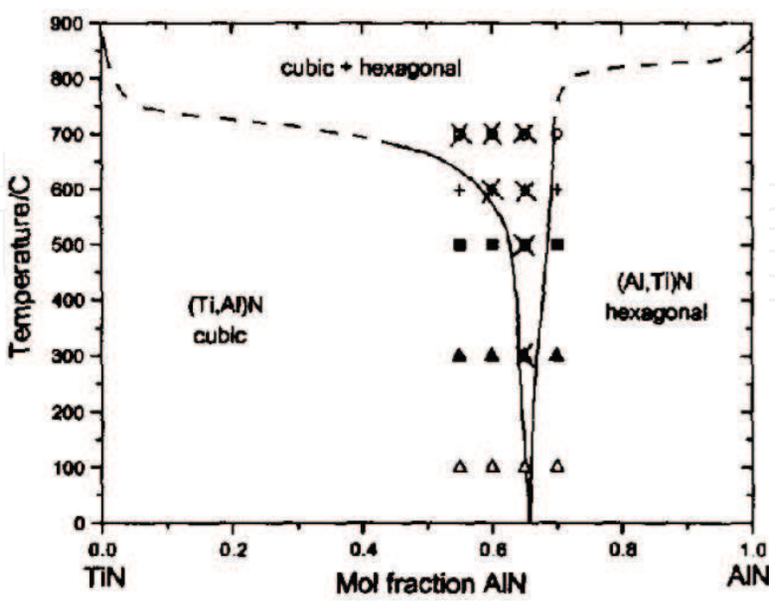

Figure 3. Metastable pseudobinary TiN-AlN diagram based on experimental results from films obtained by magnetron sputtering up to 700°C [31] (from experimental study in [30]).

2.2.3. The spinodal nature of the Ti-Al-N system

As previously enounced, thermodynamical and ab initio calculations have clearly shown the spinodal nature of the Ti-Al-N system. They also demonstrated that this spinodal decomposition occurs in a wide range of temperature. In their study concerning demixing behavior of the fcc-$Ti_{1-x}Al_xN$ structure, Mayrhofer et al. [32] have notably found that the free energy curve of the TiN-AlN mixture shows the presence of the spinodal decomposition up to 4000°C (**Figure 4**). Thus, the existence of the $Ti_{1-x}Al_xN$ solid solution is thermodynamically not possible up to this temperature. However, recent calculations of a metastable phase diagram taking into account the influence of the lattice vibrations due to temperature on free energy of the fcc-$Ti_{1-x}Al_xN$ structure showed a considerable reduction of maximum temperature of the demixing domain [33]. Nevertheless, this calculated temperature (≈2600°C) is still higher than the common temperature range used for deposition of coatings by CVD methods (600–1800°C).

Calculations are also focused on the chemical spinodal nature of Ti-Al-N in order to explain why the solid solution fcc-$Ti_{1-x}Al_xN$ remains stable up to 700°C. Actually, spinodal decomposition is distinguished from nucleation and growth by the spontaneous isostructural demixing [19]. The total free energy evolutions, associated to the spinodal decomposition, depend on several factors, as shown in the Eq. (1) [34]:

$$\Delta G = \frac{1}{2}\frac{d^2G}{dc^2}\Delta c^2 + \frac{K}{\lambda^2}\Delta c^2 + \frac{E}{1-\nu}\eta^2 V_m \Delta c^2 \tag{1}$$

where Δc is the compositional variation $c - c_0$, λ, the period of the compositional fluctuations, K, a constant that depends on the bonding energy of the atoms, E, the Young's modulus, ν, the Poisson's ratio, η, the lattice mismatch per unit of compositional variations $\eta = (1/a)(da/dc)$, and V_m, the molar volume. The first term refers to the change in free energy associated to the

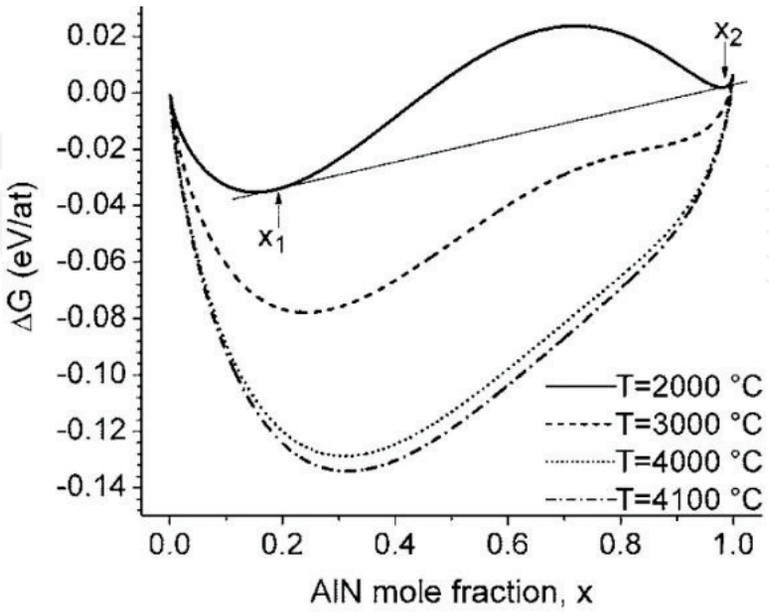

Figure 4. ΔG curve of the TiN-AlN mixture as a function of the AlN content for different temperatures [32].

decomposition, the second term describes the compositional fluctuations inside the material and represents then the driving force for the spinodal decomposition, and the last term is related to the strain energy associated to the formation of the two domains resulting from spinodal decomposition. During spinodal decomposition, the compositional fluctuations inside the material are amplified to form two isostructural phases with coherent or incoherent interfaces [35]. However, the formation of these interfaces is accompanied by strain energy, related to the lattice parameter misfit between the two phases formed after demixing (about 200–500 mJ/m^2 for a coherent interface and 500–1000 mJ/m^2 for incoherent interfaces). According to the Hilliard and Cahn theory [34, 36], if this strain energy is sufficiently large, it is able to balance the driving force for spinodal decomposition (i.e., compositional fluctuations) and then, able to hinder spinodal decomposition. Thus, Zhang et al. show that spinodal decomposition in the Ti-Al-N system occurs exclusively if coherent domains are formed [34, 36]. This phenomenon is responsible of the age-hardening effect observed in $Ti_{1-x}Al_xN$ coatings. The relationship between the spinodal decomposition parameters (especially the wavelength of the compositional fluctuations) and the microstructure of the Ti-Al-N coatings was recently studied by mean of the Calphad technique with good agreement with the experimental results obtained in the literature [37].

Alling et al. [38] studied the effect of pressure on the stability of the B1 structure. On one hand, they found that contact pressure of 20 GPa gives a weak increase of the isostructural mixing enthalpy for the fcc structure and then enhances slightly the spinodal decomposition. On the other hand, the pressure leads to a significant reduction of the mixing enthalpy of fcc and hcp structures and thus should delay the formation of the detrimental hexagonal structure for Al-rich fcc-$Ti_{1-x}Al_xN$ during operations as machining, where coatings are subjected to high temperatures and pressures.

2.2.4. Thermal stability

As a metastable phase, the fcc-$Ti_{1-x}Al_xN$ solid solution tends to return to its stable state when temperature increases. The annealing process under vacuum thus leads to decomposition of the solid solutions, firstly by spinodal decomposition to form the two coherent fcc domains and then by nucleation of hcp-AlN. The spinodal decomposition is otherwise not always observed during annealing experiments and stable phases fcc-TiN and hcp-AlN can be directly formed, depending on annealing process [28]. Furthermore, the observation of the two cubic TiN and AlN phases, as a result of the spinodal decomposition, can be difficult due to the close position of some fcc-AlN X-ray diffraction responses with those of fcc-TiN. Recent studies on the coefficient of thermal expansion of $Ti_{1-x}Al_xN$ and CrAlN coatings have shown that the presence of the B4 structure (hcp-$Ti_{1-x}Al_xN$ or hcp-AlN) in the as-deposited state promotes the further formation of these hexagonal phases during annealing [9].

The decomposition process is, as oxidation and hardness, highly dependent to the aluminum content of the as-deposited coatings. Studies show that films with high aluminum contents, and thus having a higher demixing energy than that of films with low aluminum contents, tend to decompose at lower temperature [23, 28]. However, depending on annealing parameters, the strain energy needed to the formation of the two cubic domains can retard the

spinodal decomposition and then can increase the stability of the coating. Typically, the decomposition of the solid solution occurs at temperatures between 700 and 900°C, depending on the aluminum content in the as-deposited coating [23, 39]. LPCVD $Ti_{1-x}Al_xN$ coatings with aluminum content of about x = 0.8 deposited by Endler in 2008 have shown a particularly high stability, with the first signs of decomposition at 1200°C [27]. The reasons for this exceptional stability under vacuum conditions are not clearly defined. An increase of the thermal stability of $Ti_{1-x}Al_xN$ coatings can be achieved by adding elements as Si, Hf, or Ta [40–42].

3. Deposition of $Ti_{1-x}Al_xN$ coatings

3.1. Crystallographic structure

As briefly described earlier in the thermodynamical description of the Ti-Al-N system, as-deposited $Ti_{1-x}Al_xN$ coatings have commonly three distinct structures: fcc, hcp, and a mix of fcc and hcp. These crystallographic structures are obtained for both PVD and CVD coatings and show a strong dependence on the aluminum content. For lower aluminum content, aluminum atoms are considered to replace titanium atoms in the fcc-TiN structure and form the single-phase fcc-$Ti_{1-x}Al_xN$. This phase is the desired one on tools for cutting operations, needing high hardness, high thermal stability, and good oxidation resistance.

By increasing aluminum content in the films, a biphased structure appears. These phases are cubic (fcc) and hexagonal (hcp), but their compositions depend on the deposition process. Concerning PVD processes, for which condensation of a vapor on a cold substrate occurs, the cooling rate are so high that deposition of metastable materials is expected. A mixture of fcc-$Ti_{1-x}Al_xN$ and hcp-$Ti_{1-x}Al_xN$ can be observed, as reported by Chen et al. [23] for magnetron sputtered coatings deposited at 500°C and a working pressure of 0.4 Pa. These results are in agreement with the metastable diagram established by Cremer et al. (**Figure 3**). Concerning the thermal CVD process, performed at high temperatures and then closer to the thermodynamic equilibrium, a mixture of the stable phases fcc-TiN and hcp-AlN is generally reported [23, 27]. The presence of fcc-AlN, in addition to the fcc-TiN and hcp-AlN phases, was also found by Wagner et al. for APCVD coatings, forming a three-phase structure. The fcc-AlN formation was attributed to the spinodal decomposition of the fcc-$Ti_{1-x}Al_xN$ coatings, where an excess of Al atoms in the fcc-$Ti_{1-x}Al_xN$ solid solution leads to an increase of the demixing energy and then cause the formation of fcc-AlN [43]. The aluminum content threshold, at which this crystallographic transition occurs, depends on the deposition techniques and process parameters (up to about x = 0.7 for PVD and up to x = 0.9 for CVD and PECVD). Anyway, the presence of a mixture of these two phases is generally detrimental for both mechanical properties and oxidation resistance of the films [7, 25, 26], except if a nanocomposite is formed [44, 45]. This mixing of hcp and fcc structures remains up to x = 1 for coatings deposited by CVD and PECVD processes [27, 44–46]. It should be noted, however, that the achievable microstructures for LPCVD processes are a little bit more complex and very dependent of process parameters. As denoted above, even though fcc-$Ti_{1-x}Al_xN$ solid solutions were found up to x = 0.9, the presence of nanocomposite structures was recently reported. The deposition

of $Ti_{0.05}Al_{0.95}N$ coatings, composed of an alternate of fcc-TiN/hcp-AlN nanolamellae embedded in a Al-rich $Ti_{1-x}Al_xN$ was thus found by Keckes et al. in 2013 [44]. More recently, nanocomposite structures constituted by Ti-rich fcc-$Ti_{1-x}Al_xN$/Al-rich fcc-$Ti_{1-x}Al_xN$ nanolamellae (for $0.73 < x < 0.82$) were also deposited in an industrial CVD facility [44, 47–49].

In the case of PVD, the deposition of a single-phase hcp-$Ti_{1-x}Al_xN$ is observed for aluminum contents above $x \approx 0.7$. This phase is generally found to be detrimental for mechanical properties and oxidation resistance but some researchers found a better oxidation resistance for these hcp-$Ti_{1-x}Al_xN$ coatings deposited by unbalanced magnetron sputtering [23].

These microstructural changes are summarized in **Figure 5**. The structure obtained for different deposition processes (PVD, PECVD, and thermal CVD), associated to their out-of-equilibrium level, is defined as a function of the aluminum content in the $Ti_{1-x}Al_xN$ coatings. As fcc-$Ti_{1-x}Al_xN$ is a metastable phase, we could expect that higher aluminum content should be obtained for the process with the highest out-of-equilibrium level, so for PVD processes. However, as described above, higher aluminum content in the fcc phase is obtained for LPCVD and PECVD processes. Atmospheric pressure CVD (APCVD) process, near to the thermodynamic equilibrium, leads to relatively low aluminum contents in the fcc-$Ti_{1-x}Al_xN$ phase (about $x = 0.4$) [43].

3.2. Physical vapor deposition (PVD) of $Ti_{1-x}Al_xN$ coatings

Vacuum cathodic arc deposition (CAD) process [50–53] is probably the most widely used PVD technique on an industrial scale to prepare protective hard $Ti_{1-x}Al_xN$-based coatings on cutting tools and forming molds [50, 54, 55]. The high ionization levels of cathodic arc

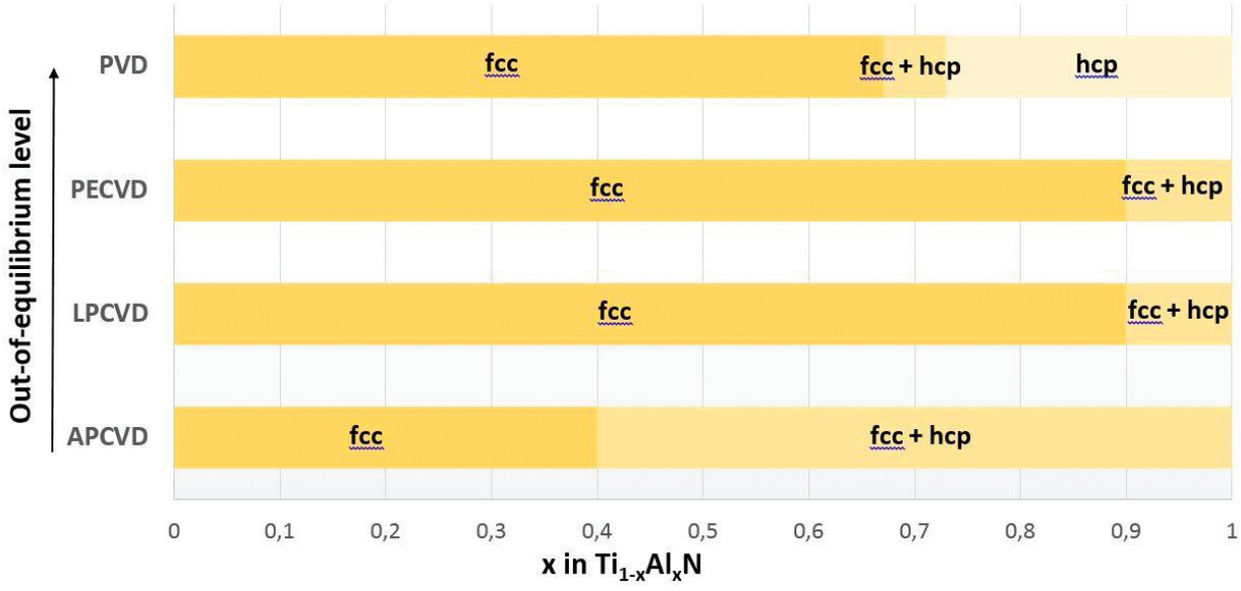

Figure 5. Crystallographic structures of $Ti_{1-x}Al_xN$ coatings obtained for APCD, LPCVD, PECVD, and PVD processes according to the aluminum content. "fcc" is related to the fcc-$Ti_{1-x}Al_xN$ solid solution; "fcc + hcp" refers to a mix of fcc-$Ti_{1-x}Al_xN$ + hcp-$Ti_{1-x}Al_xN$ for PVD coatings and to fcc-TiN + hcp-AlN for CVD and PECVD coatings; "hcp" refers to the hcp-$Ti_{1-x}Al_xN$ solid solution (data from [23, 27, 43, 46]).

discharges and high ion energy can provide advantages such as enhanced adhesion required for mechanical applications involving high loads. CAD allows deposition of a wide range of hard compounds as nitrides or carbonitrides. However, CAD is also often associated to macrodroplet generation that degrades the surface roughness of coatings. Droplets' density in the films, which is not redhibitory for cutting operations, has been significantly reduced thanks to the development of high-performances cathodes. The current trend is to develop advanced nanostructured hard coatings in order to enhance properties as hardness, toughness, and oxidation resistance [54, 55]. The deposition of $Ti_{1-x}Al_xN$ coatings by various PVD methods was hugely documented since several decades. Then, this review will focus mainly on CVD coatings and particularly on the thermal CVD process.

3.3. Chemical vapor deposition (CVD) of $Ti_{1-x}Al_xN$ coatings

Thermal CVD deposition process is based on thermodynamic aspects, fluid mechanics, related to the transport of gaseous precursors toward the substrates and kinetics of deposition, allowing to synthetize metastable phases. Adjusting these parameters allows reaching a large range of microstructure and morphologies. For example, the stabilization of the metastable fcc-$Ti_{1-x}Al_xN$ is the result of a low mobility of species at the substrate surface. Thus, low temperatures, high partial pressure, and low total pressure are required. Processes as LPCVD and PECVD are now widely used in industrial plants for deposition of aluminum-rich Al-Ti-N coatings. However, MOCVD processes remain rare, because of the highly volatile nature and the high cost for preparing metalorganic precursors. Thus, regarding the lack of extended literature on MOCVD $Ti_{1-x}Al_xN$ coatings, the following parts will mainly focus on thermal CVD and PECVD processes. Anyway, studies on MOCVD processes and specific precursors are available in [21, 56–58].

3.3.1. Gaseous reactions

Although the deposition of $Ti_{1-x}Al_xN$ coatings is widely performed by PVD and PECVD processes, it is less common by thermal CVD processes. The good understanding of the process needs to take into account a lot of parameters linked to thermal homogeneity and distribution of gases. A detailed description of the fluid mechanics and thermic mechanisms inside the reactor related to chemical vapor deposition systems is given in [59–63]. Here, we briefly describe the gases production and reactions leading to the formation of coatings in the Ti-Al-N system.

Deposition of TiN and AlN by thermal CVD is generally performed using metal chlorides as $TiCl_4$ and $AlCl_3$. Gaseous $TiCl_4$ is often generated with a bubbler by adjusting vapor pressure in the $TiCl_4$ tank but systems regulating directly the liquid flow of $TiCl_4$ also exist. $AlCl_3$ is typically generated by in situ chlorination by passing HCl through Al platelets. Anderbouhr et al. [64, 65] have also demonstrated the possibility to deposit $Ti_{1-x}Al_xN$ coatings from $TiCl_3$ and $AlCl_3$ generated by passing Cl_2, HCl, or $TiCl_4$ on Ti-Al bulk alloys. However, the chlorination conditions (temperature and pressure) could generate unwanted species, and particularly solid <$TiCl_2$> that precipitates below about 700°C [64]. This range of temperature is in the common range used for generation of aluminum chlorides (300–400°C), in order to generate

only $AlCl_3$ and its dimer Al_2Cl_6 species. Thus, the direct chlorination of TiAl has to be realized at temperatures above 700°C. The nitrogen source was initially N_2, for the deposition on carbide tools. NH_3 is now commonly used, notably due to the development of microelectronics industry. The lower stability of NH_3 compared to that of N_2 allows to react with $TiCl_4$ and $AlCl_3$ at lower temperatures.

As previously said, the formation of the fcc-$Ti_{1-x}Al_xN$ solid solution is envisioned to be the result of the codeposition of the metastable fcc-AlN and stable fcc-TiN. The reaction process using NH_3 is considered to result mainly from the reactions (2) and (3):

$$6TiCl_4 + 8NH_3 \rightarrow 6TiN + 24HCl + N_2 \quad (2)$$

$$AlCl_3 + NH_3 \rightarrow AlN + 3HCl \quad (3)$$

Other intermediate reactions forming complex molecules should also occur in the reactor and in the exhaust system but their formation seems mainly to occur for APCVD process [66, 67].

3.3.2. Morphology/microstructure

Thermal CVD deposition is highly dependent on the total pressure, partial pressure of precursors, as well as on the deposition temperature. An overall description of the effects of these parameters could be summarized as follows [59, 68] and shown in **Figure 6**:

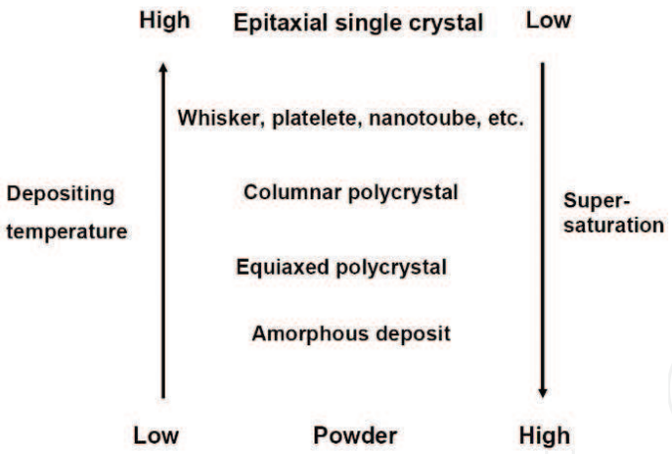

Figure 6. Summary of the typical microstructure of CVD coatings with regards to the deposition temperature and the supersaturation [59].

- High temperatures during deposition promote surface diffusion and adatom mobility, leading to coarsening of the grains.
- In the same way, a low partial pressure (or a low supersaturation) allows better surface mobility of atoms and then leads to coarse grains. Epitaxial coatings are then obtained for high deposition temperatures and low partial pressure. High partial pressure and low temperature rather give nanosized grains or amorphous coatings.

- The total pressure acting mostly on the diffusion in the boundary layer, a low total pressure promotes diffusion in the boundary layer and the mass transport to the surface, according to the Grove's model [59]. Then, a higher supersaturation should be achieved by lowering the working pressure.

Other parameters as distance of the substrate from gas inlet or discharge voltage for PECVD techniques have also to be taken into account to optimize the morphology/microstructure of the coatings.

TiN coatings obtained by CVD processes show generally columnar growth, according to the Van der Drift model [69], and resulting from the competition between different crystalline orientations. In fact, growth of grain is thermodynamically more favorable along some orientations: the grains having these favorable orientations perpendicularly to the substrate surface will be favored and will lead to column formation [69]. The preferential orientation depends strongly on the process parameters (gas ratios, deposition temperature, partial pressure of each precursors, etc.). As an example, for TiN coatings deposited at atmospheric pressure, Cheng et al. found, at high temperature and high N_2 partial pressure, a (200) texture while they found a (110) texture at low temperature and high N_2 partial pressure [70, 71]. In the same way, the control of process parameters allows to achieve a wide range of morphologies [68]. Thus,

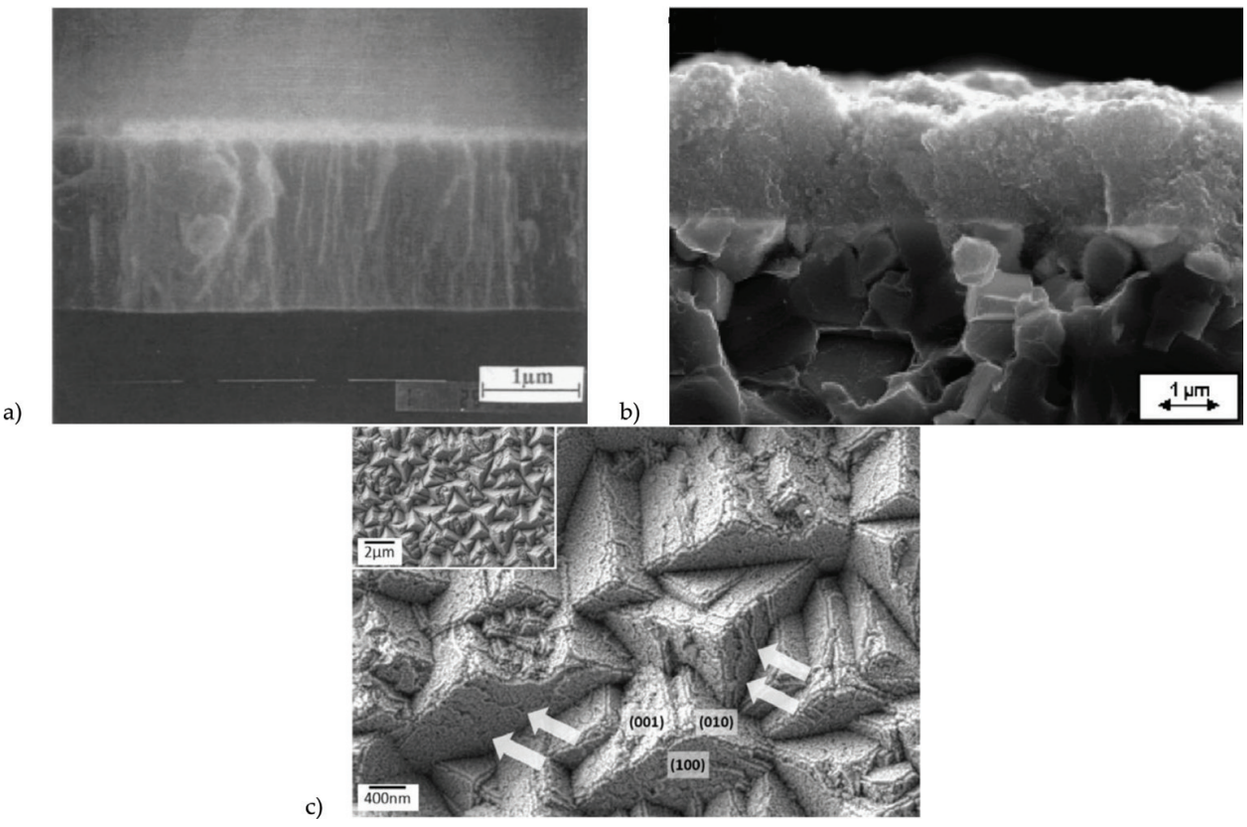

Figure 7. Microstructure of $Ti_{1-x}Al_xN$ coatings for different aluminum content: (a) columnar structure of $Ti_{0.92}Al_{0.08}N$ deposited on silicon substrate by LPCVD [65]; (b) agglomerate-like structure of $Ti_{0.23}Al_{0.72}N$ deposited on WC/Co substrate by APCVD [43]; (c) nanocomposite fcc-$Ti_{1-x}Al_xN$/Al-rich fcc-$Ti_{1-x}Al_xN$ arrangement forming cubes having the (111) planes parallel to the surface [48].

microstructures like agglomerate-like grains, lenticular-shaped grains, or star-shaped grains were reported [70, 72–76].

In the case of $Ti_{1-x}Al_xN$, a strong dependence to Al content and process parameters is observed. Thus, Anderbouhr et al. have deposited $Ti_{1-x}Al_xN$ films by LPCVD in a laboratory scale unit at temperatures from 600–1000°C and a pressure of 1130 Pa [64]. They found fine columnar morphology (**Figure 7a**) up to x = 0.2 and glassy morphology for the highest aluminum contents (x ≈ 0.7). Wagner et al. have deposited $Ti_{1-x}Al_xN$ up to x = 0.72 in an industrial thermal CVD unit and at atmospheric pressure [43]. As it should be seen in **Figure 7b**, they also found columnar growth for low Al contents (single-phased fcc-$Ti_{1-x}Al_xN$ structure) but coarse agglomerate-like structure for highest value of x (biphased fcc-TiN/hcp-AlN structure). These results confirm the influence of working pressure on grain coarsening: the LPCVD process allows achieving higher supersaturation on the surface of the growing film and then leads to a grain refinement. These coatings have generally no preferential orientation. However, the recent deposition of $Ti_{0.18}Al_{0.82}N$ nanocomposites reveals the particular formation of "cubes," growing with the [111] direction perpendicular to the substrate surface (see **Figure 7c**). XRD analysis revealed the presence of both Al-rich fcc-$Ti_{1-x}Al_xN$ and Ti-rich fcc-$Ti_{1-x}Al_xN$ solid solutions. Further TEM analysis revealed the presence of coherent Ti-rich fcc-$Ti_{1-x}Al_xN$/Al-rich fcc-$Ti_{1-x}Al_xN$ nanolamellae. The lattice accommodation between these lamellae was attributed to the self-adjustment of the Ti, Al, and N concentration near the interface [48]. PECVD coatings also show a grain refinement with increasing aluminum incorporation [28, 46, 77]. Other parameters have to be taken into account in order to describe coatings' morphologies obtained by PECVD processes. An increase of the gas inlet distance seems to lead to a fine-grain morphology. This evolution should be related to the increase of the aluminum content and the drop of the nitrogen content in the coatings. The higher gas inlet distance leads to substoichiometric coatings (only 35 at% of nitrogen in the coatings instead of the 50 at% for stoichiometric coatings) and showing a mixture of fcc-$Ti_{1-x}Al_xN$ and hcp-$Ti_{1-x}Al_xN$ phases [46]. Discharge voltage does not seem to influence directly the morphology of coatings but influences the aluminum content.

3.3.3. Chemical composition and crystallographic structure

Chemical composition is one of the most important characteristics in $Ti_{1-x}Al_xN$ coatings due to its strong influence on the crystallographic structure. Since the crystallographic structure is highly dependent on the aluminum content, researches led on $Ti_{1-x}Al_xN$ coatings focused mainly on the optimization of the aluminum content in the films, particularly in the fcc structure, allowing to reach the particular mechanical and chemical properties of $Ti_{1-x}Al_xN$ films.

3.3.3.1. Aluminum content

Although the deposition of $Ti_{1-x}Al_xN$ coatings is widely performed by PVD processes, it is less common by PECVD and thermal CVD processes. Thus, PVD fcc-$Ti_{1-x}Al_xN$ single-phased coatings are limited to x = 0.67–0.7. As an example, the single-phase fcc-$Ti_{1-x}Al_xN$ was obtained up to x = 0.67 in films deposited by magnetron sputtering [23], up to 0.65 by

cathodic arc deposition [78, 79] and up to 0.71 by high-power impulse magnetron sputtering (HiPIMS) [80]. This limit is consistent with the metastable solubility limit predicted by thermodynamic and ab initio calculations. In contrast, CVD processes allow to deposit fcc structure with higher aluminum contents. Even though the possibility to deposit fcc-$Ti_{1-x}Al_xN$ at atmospheric pressure (APCVD) and at relatively low temperatures (<700°C) was demonstrated by Wagner et al. [43], the morphological aspects of the coatings and the associated bad mechanical properties for high aluminum contents lead to some limitations for APCVD processes. It seems thus difficult to deposit performant $Ti_{1-x}Al_xN$ coatings by APCVD with an aluminum content higher than 0.4. However, LPCVD development has led to achieve deposition of aluminum-rich coatings with good mechanical properties and having aluminum contents higher than that reached at atmospheric pressure. Anderbouhr et al. have thus shown the possibility to deposit the fcc-$Ti_{1-x}Al_xN$ solid solution up to $x \approx 0.7$ by a LPCVD process using titanium and aluminum chlorides [64, 65]. Later, Endler et al. obtained fcc-$Ti_{1-x}Al_xN$ up to $x = 0.9$ at 800°C and pressure < 10 KPa [27]. Fcc-$Ti_{1-x}Al_xN$ coatings with $x \approx 0.8$ and deposited at pressure below 50 mbar are notably industrially used [81]. These CVD coatings were deposited with $AlCl_3/TiCl_4$ gas ratio > 1, due to the higher stability of $AlCl_3$ than that of $TiCl_4$. An increase of the $AlCl_3/TiCl_4$ ratio leads to a rise of the aluminum content in the coating [27, 43, 64]. As shown in **Figure 8**, the same dependence is observed for PECVD coatings [28, 29]. As specified previously, discharge voltage and gas inlet distance from the substrate strongly influence the chemical composition. Increasing discharge voltage favors aluminum incorporation in the coatings [28, 46]. In the same way, increasing distance from gas inlet strongly increases the aluminum content and, as a consequence, leads to granular microstructure [46].

The reason for the huge gap between the metastable solubility limits of aluminum in the fcc-TiN structure obtained for different deposition processes (around 0.7 for PVD, 0.9 for LPCVD and PECVD methods) is only poorly discussed in literature. However, Mayrhofer et al. [82] led ab initio calculations to study the influence of the distribution of Al atoms substituting Ti in the

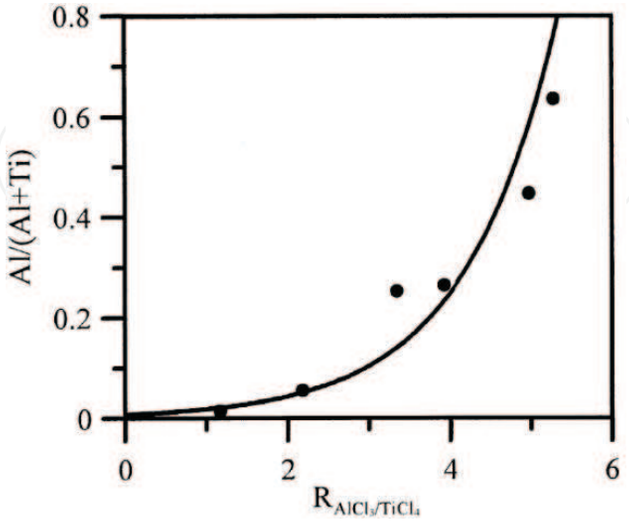

Figure 8. Evolution of the aluminum content in the $Ti_{1-x}Al_xN$ coatings vs. $AlCl_3/TiCl_4$ ratio for PECVD coatings deposited at 500°C and about 670 Pa [83].

fcc-TiN structure. They found that the aluminum distribution giving the lowest quantity of Ti-Al bonds led to high solubility limit. Their results showed notably an increase of the solubility limit from x = 0.64 to x = 0.74 only by changing the atomic distribution of Al and Ti. Thus, they concluded that the distribution of the aluminum atoms in the lattice is one of the factors explaining the high solubility limit obtained for PECVD and LPCVD coatings.

3.3.3.2. Impurities

Another factor that should influence properties of the coatings is the chlorine incorporation after CVD deposition. Concerning CVD process, for which the temperature is the key factor, higher deposition temperatures promote precursor dissociation and thus lead to a decrease of the chlorine content in the coatings. However, a rise of the aluminum precursor flow rate leads to an increase of the Cl content in the film [43, 77, 83]. Concerning PECVD process, an increase of the discharge voltage leads to a better dissociation of species and thus reduces Cl content in the coatings [28, 46]. In the same way, increasing gas inlet distance leads to a higher dissociation of Al precursor and then to decrease the Cl content [46]. Oxygen is also generally identified as a detrimental element for the properties of the coatings. However, while several studies describe the mechanisms responsible for the oxide formation (the oxygen diffusion notably) during annealing of the $Ti_{1-x}Al_xN$ coatings, no studies were found concerning the effect of the oxygen content on the properties of the coatings (except the oxide scale formation).

4. Properties of $Ti_{1-x}Al_xN$ coatings

$Ti_{1-x}Al_xN$ coatings are now extensively used for machining applications, where good mechanical and chemical properties are needed in order to ensure the stability of the coatings in in-service conditions. These properties are strongly dependent on the chemical composition of the coating and the working temperature, which could lead to a change in structure of the coating. Properties as hardness and oxidation resistance are then reviewed with respect to the aluminum content in the fcc-$Ti_{1-x}Al_xN$ phase and deposition temperature.

4.1. Mechanical properties

4.1.1. Hardness

4.1.1.1. Al-content dependence of hardness

Hardness of the coating is a key property for increasing the wear resistance and improving the tool lifetime of the cutting tools. The hardness of coatings is generally characterized by mean of nanohardness tests. Among the mechanical properties of $Ti_{1-x}Al_xN$ coatings, the hardness is only indirectly related to the aluminum content via the crystallographic structure. Thus, an increase of the aluminum content in the fcc-$Ti_{1-x}Al_xN$ phase leads to an increase of the hardness. The main mechanism is solid solution hardening: the substitution of Ti by Al atoms in the fcc-TiN leads to a lattice distortion and thus limits the motion of

dislocations [28]. Above an aluminum content threshold, a mixture of two phases, the cubic and hexagonal structures, is deposited. The presence of the hcp phase, observed for about x = 0.7 in $Ti_{1-x}Al_xN$, leads to a drop in hardness of the coatings [8, 23], as it can be seen in **Figure 9**. Highest aluminum contents lead, as specified earlier, to the deposition of hcp-$Ti_{1-x}Al_xN$ single-phased coatings, when a PVD method is used, associated with lower hardness. The hardness of some coatings deposited by PVD, CVD, and PECVD methods related to the structure and process parameters is summarized in the table given in Appendix A. It can be seen that PVD $Ti_{1-x}Al_xN$ monolayer coatings generally show hardness between 25 and 30 GPa. Concerning CVD processes, for which the aluminum content in the fcc-$Ti_{1-x}Al_xN$ solid solution can reach values up to x = 0.9, hardness up to 32.4 GPa was reported. Nanocomposite structures consisting of an alternate of fcc and hcp nanolamellae were found to have a relatively high hardness (≈26 GPa) compared to other hcp-AlN-containing coatings [45]. Higher hardness (36 GPa) was then obtained for fcc-$Ti_{1-x}Al_xN$/Al-rich fcc-$Ti_{1-x}Al_xN$ nanocomposites [47]. PECVD techniques, due to their high out-of-equilibrium nature, also allow to deposit coatings which are fcc-$Ti_{1-x}Al_xN$ single-phased with x values up to ≈0.91, as reported by Prange et al. [28]. The highest hardness of single-phased coatings in this study was found for the fcc-$Ti_{0.17}Al_{0.83}N$ with value of 38.7 GPa. Coatings with aluminum content higher than 0.91 were deposited and hardness up to 5000 HV (≈49 GPa) was reached. However, this huge increase in hardness is mainly attributed to the biphased nanocrystalline structure associated with a significant grain refinement. The large range of hardness observed for these different deposition processes can be explained by the high dependence of hardness to many parameters as the grain size (according to the Hall-Petch law), residual stresses, morphology, and structure of coatings [28, 84–87].

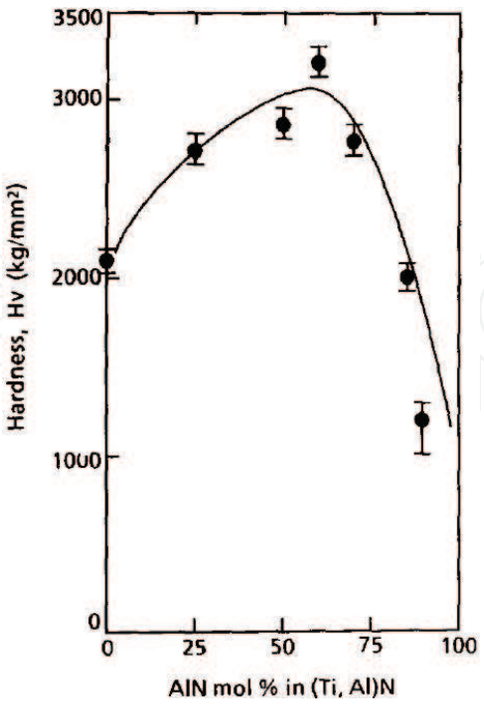

Figure 9. Evolution of hardness vs. aluminum content in coatings deposited by cathodic arc ion plating [25].

http://dx.doi.org/10.5772/intechopen.79747

4.1.1.2. Temperature dependence of hardness

The nitrides, like TiN, show a sharp decrease in hardness at temperatures above 400°C, because of mechanisms as restauration and recrystallization [19]. However, alloying with elements theoretically immiscible in TiN like aluminum allows changing completely the temperature dependence of the hardness. The evolution of the hardness as a function of temperature is related to the thermal stability of the material and to its decomposition process. The coherent spinodal nature of the decomposition of fcc-$Ti_{1-x}Al_xN$ can only lead to the formation of fcc-TiN and fcc-AlN with coherent interfaces, where the lattice mismatch allows hindering the dislocations' movement and so resulting in an increase of hardness. This behavior is responsible of the so-called age-hardening effect observed in $Ti_{1-x}Al_xN$ coatings. However, the peak of hardness is not observed at the same temperature for all coatings but depends also on the aluminum content in the films. Thus, an fcc-$Ti_{1-x}Al_xN$ coating with aluminum content close to the apparent solubility limit (for example, 0.7 for PVD coatings) has higher demixing energy than coatings with lower aluminum contents and has a trend to decompose more easily, as predicted by thermodynamical and ab initio calculations [29]. These calculations are in agreement with experimental studies showing that the age-hardening occurs earlier for Al-rich coatings. Chen et al. [23] have thus led a study of the mechanical properties and thermal stability of $Ti_{1-x}Al_xN$ coatings deposited by unbalanced magnetron sputtering process at 500°C, 0.4 Pa, and bias voltage of −60 V. They clearly show that the temperature corresponding to the maximum hardness decreases when Al content increases. This behavior is shown **Figure 10**.

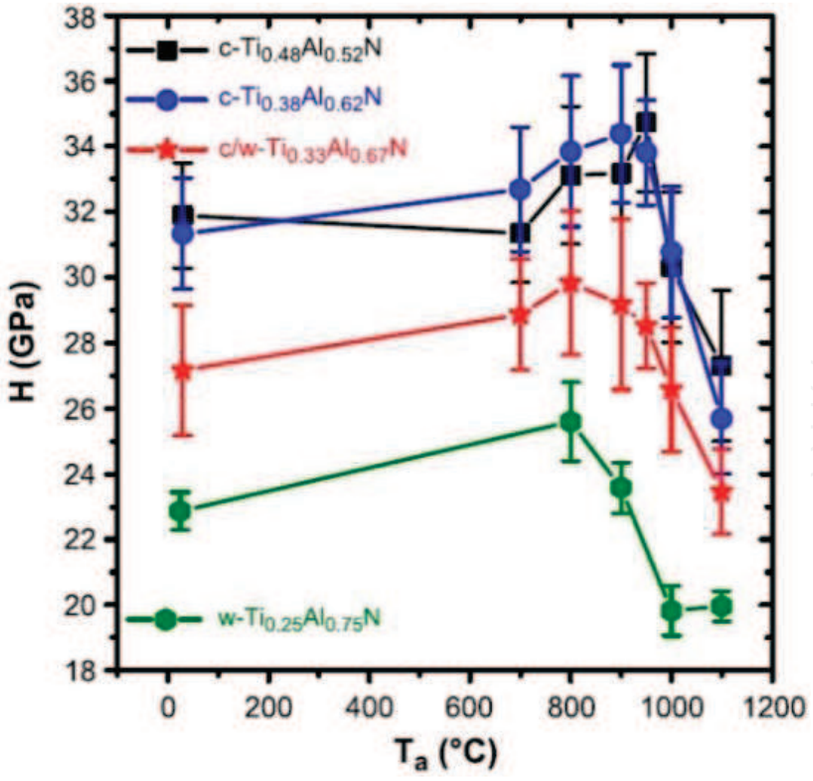

Figure 10. Evolution of hardness vs. annealing temperature for coatings with different aluminum contents deposited by unbalanced magnetron sputtering [23].

It is also important to note that an enhancement of the hardness with temperature was also observed in this study for an hcp-$Ti_{0.25}Al_{0.75}N$ single-phased film [23]. Based on XRD analysis, the authors proposed that this hardness enhancement is related to the formation of fcc-TiN precipitates. This age-hardening effect can also be observed for nanocomposite coatings with high hardness stable up to 1100°C, while the "standard" fcc-$Ti_{1-x}Al_xN$ solid solution coatings show a significant drop of hardness for temperatures above 1000°C [45, 47].

4.1.2. Residual stresses

Residual stresses act strongly on the mechanical properties of coatings. Compressive stresses lead to better wear resistance, especially for adhesive wear at high temperature, by reducing diffusion in the coating. However, a too high level of compressive stress can lead to cohesive and/or adhesive spalling. For this reason, studies aim generally at obtaining coatings with the smallest residual stresses. CVD coatings show generally lower residual stresses than PVD coatings because of the atomic peening of the growing film, which leads to local densification and so, to additional compressive stresses in PVD coatings.

Residual stresses are decomposed into two contributions: the thermal stresses, related to the difference of coefficient of thermal expansion between the substrate and the coating; and the intrinsic stresses, related to the process parameters and to morphology. The flux and kinetic energy of species in the PVD processes, particularly those involving high ionization discharges, can generate a local densification of the coating (atomic peening), leading to compressive stresses, while, under low bombardment conditions, a columnar growth is associated to tensile or low compressive stresses, depending on the intercolumnar distance, according to the Hoffman model [88].

Residual stresses are generally measured using the substrates' curvature technique and calculated by the Stoney's formula. Values obtained in different studies are difficult to compare because of the strong dependence to many factors. First, the "material" factors such as thickness of coating, texture, presence of underlayer as TiN [27], TiAl, $Ti_{1-x}Al_xN$ with gradual Al content [89], or nature of substrate influence strongly the residual stresses after deposition. Moreover, process parameters also play a role in the evolution of stresses, as deposition temperature or bias voltage [90]. Ahlgren et al. [90] have thus shown that increasing the bias voltage during the deposition of arc deposited $Ti_{1-x}Al_xN$ leads to a significant increase of the residual stresses in the coating. Stresses of −1.69 GPa were then obtained for a bias voltage of −40 V, while values of −5.59 GPa were found at bias voltage of −200 V.

Shum et al. led a structural and mechanical study of $Ti_{1-x}Al_xN$ films with respect to the Al content [91]. The films were deposited by reactive close-field unbalanced magnetron sputtering and high compressive stresses (≈ − 3 GPa) were measured for TiN. This result was related to the low deposition pressure of 0.27 Pa, which favors an intense bombardment of the growing film. They found that Al incorporation up to x = 0.41 leads to a significant decrease of the residual stresses (**Figure 11**). For this Al content, the lowest compressive stresses of about −0.35 GPa were measured and they attributed these results to the presence of amorphous AlN around $Ti_{1-x}Al_xN$ grains. When aluminum content is further increased, the residual stresses rise up to value of ≈ − 1.5 GPa for pure AlN (**Figure 11**). This behavior was linked to the increasing fraction of hcp-AlN.

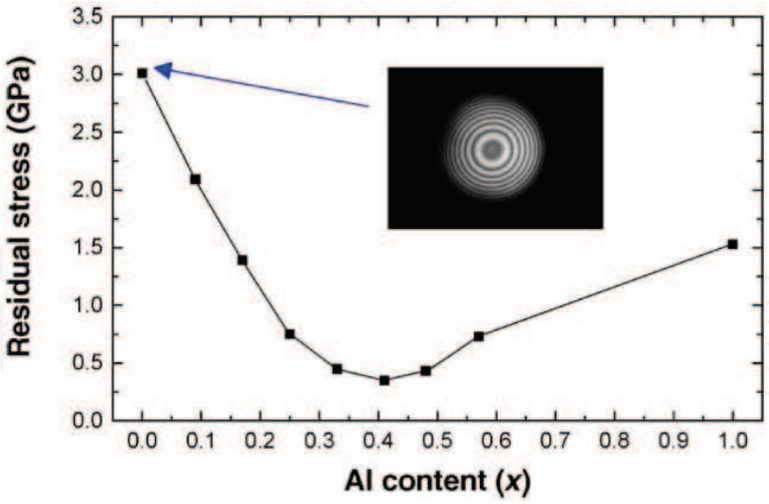

Figure 11. Evolution of the residual stresses vs. aluminum content in $Ti_{1-x}Al_xN$ thin films deposited by reactive unbalanced magnetron sputtering [91].

PVD coatings deposited on WC/Co carbides show compressive stresses between −1 and − 5 GPa [26, 90] and values above 5 GPa are reported to cause delamination of the film deposited by cathodic arc deposition [90]. Concerning thermal CVD coatings, Endler et al., who deposited fcc-$Ti_{1-x}Al_xN$ single-phased films with x = 0.82 on WC/Co obtained compressive stress less than 1 Gpa, partly due to the presence of a TiN sublayer [27]. The residual stresses measured on coatings obtained by different deposition techniques are summarized in the table in Appendix A.

4.2. Oxidation resistance

4.2.1. Overall mechanisms

During machining operations, cutting tools are subjected, in addition to mechanical stresses, to high temperatures, that can reach 1000°C [92], which can lead to severe oxidation and consequently to altered properties of the film. The oxidation resistance of $Ti_{1-x}Al_xN$ coatings is generally associated to the formation of a dense Al_2O_3 diffusion barrier layer that protects $Ti_{1-x}Al_xN$ against further oxidation. However, oxidation mechanisms are complex and the evolution of the structures as a function of the aluminum content has a strong influence on the oxidation behavior of the coatings. Nevertheless, although oxidation mechanisms are not now completely defined, it is widely accepted that the formation of the oxide phase is the consequence of the outward diffusion of Al associated with the inward diffusion of O [7, 93–95]. Moreover, analysis performed by RBS (and later by NRA [95]) shows that oxidation is associated to a nitrogen loss. This suggests that, in the first steps of oxidation, N is substituted by O, and oxides and/or oxinitrides such as (Ti, Al)N_xO_y are formed. With further oxidation, the composition of the system evolves progressively toward the pure Al_2O_3 and TiO_2 layers as a function of oxidation parameters. With increasing oxidation time or temperature, Ti begins to oxidize to form rutile r-TiO_2. The formation of this oxide can lead to crack formation in the Al_2O_3 protective layer, acting as diffusion paths for oxygen and leading to the complete oxidation of the coatings. Titanium atoms, by passing through these cracks, lead to the formation

of a porous and detrimental r-TiO_2 top layer [40]. The oxidation behavior is thus mainly dependent on the aluminum content in the coating and on the oxidation temperature.

4.2.2. Aluminum content dependence of oxidation resistance

Most of the studies on $Ti_{1-x}Al_xN$ coatings focus on the necessity to increase aluminum incorporation in the coatings in order to promote better oxidation resistance. Actually, a continuous decrease of the oxide thickness is observed with increasing aluminum content in the coating [23], which indicates that the oxide layer prevents the coating from further oxidation. However, the oxidation resistance seems to be more related to the crystallographic structure (fcc, hcp, or mixed fcc/hcp), which is linked to the aluminum content, rather than a direct dependence to aluminum content.

Vaz et al. have summarized the evolution of the formed oxide layer regarding the temperature and aluminum content (**Figure 12**). It was shown that oxidation resistance increases with increasing the aluminum content in the coating as long as the films remain fcc single-phased (up to x = 0.65 in this study) [24]. These results are in accordance with later experiments where oxide thickness decreased with increasing aluminum content [23, 95]. According to the results of Vaz et al., although a small amount of Ti and Al remains in the Al-rich top layer and Ti-rich sublayer, respectively, the oxides formed at high temperatures and for low aluminum content

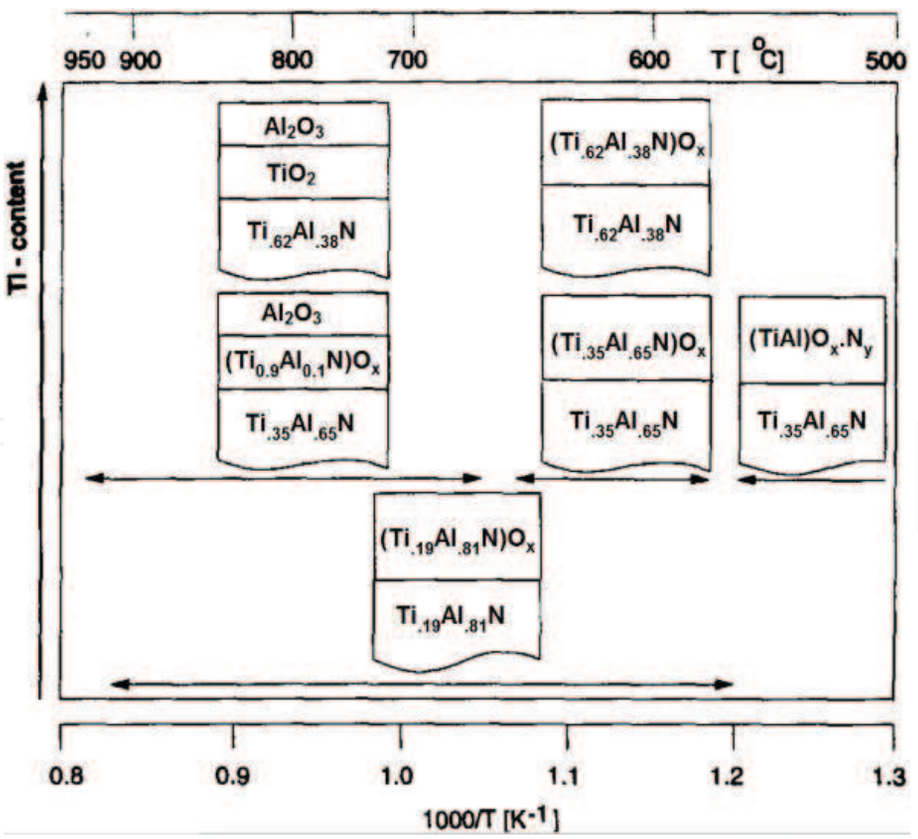

Figure 12. Schematic diagram summarized the temperature and aluminum content dependences of $Ti_{1-x}Al_xN$ coatings oxidation [24].

are assumed to be almost "pure" Al_2O_3 and TiO_2. However, with increasing x in the as-deposited fcc-$Ti_{1-x}Al_xN$ coatings, higher aluminum contents were found in the Ti-rich interlayer. Thus, this Ti-rich layer cannot be attributed to TiO_2 but rather to a mixed aluminum-titanium oxide such as $(Ti_{0.9}Al_{0.1})O_x$ oxide. Other studies also report that the oxide layer formed during oxidation at high temperature (above 800°C) is mainly composed of an $Al_xTi_yO_z$ oxide [7, 23]. These results are consistent with the higher oxidation resistance observed for Al-rich fcc-$Ti_{1-x}Al_xN$ and it suggests that higher aluminum concentration, by the formation of a dense AlO3 top layer, hinders oxygen diffusion and limits the formation of the porous and detrimental r-TiO_2.

Increasing aluminum content leads to the formation of the fcc/hcp biphased structure. Many studies show that this material has a poor oxidation resistance [24, 25]. A further increase of the aluminum content leads to the stabilization of the hcp-$Ti_{1-x}Al_xN$ or hcp-AlN (depending on the deposition temperature). These coatings were found by Vaz et al. to be totally composed of the $Al_xTi_yO_z$ oxide at 850°C. Although $Ti_{1-x}Al_xN$ coatings with hcp single-phased structure are generally found to have the worse oxidation resistance [24, 95], Chen et al. found an unexpected high oxidation resistance for hcp-$Ti_{0.25}Al_{0.75}N$ single-phased coatings [23]. CVD or PECVD coatings with fcc single-phased structure obtained for x above 0.7 seem to have a better resistance than PVD coatings (with lower aluminum content). Thus, Prange et al. found no presence of the detrimental TiO_2 for $Ti_{0.21}Al_{0.79}N$ coatings oxidized at 800°C during 1 h [28], while $Ti_{0.18}Al_{0.82}N$ coatings deposited by LPCVD were found to oxidize only at temperatures above 900°C [27]. Similar results were obtained for hcp/fcc $Ti_{0.05}Al_{0.95}N$ nanocomposite coatings, with the first signs of Al_2O_3 and TiO_2 at a temperature of 950°C [45].

4.2.3. Temperature dependence of oxidation resistance

According to the results of Vaz et al. [24], coatings oxidized at lowest temperatures (below 600°C) are only composed of titanium-aluminum oxinitrides, while, for coatings oxidized at higher temperatures, $Ti_{1-x}Al_xO_y$ oxides are observed [96]. These experiments confirm that, at the lowest temperatures, only a part of the nitrogen atoms are "substituted" by oxygen and escapes through the gas phase by forming N_2. The Ti and Al contents were also found to be the same than that of the as-deposited coatings, annealed at low temperature. However, high temperatures favor the formation of Al_2O_3 and the Al and Ti contents in this oxide layer tend obviously to be different than that of the as-deposited coatings.

4.3. Wear resistance

4.3.1. General wear mechanisms

The wear aspects take a large place in the research on hard coatings. During machining, wear is the consequence of a combination of mechanical and chemical solicitations. The wear mechanisms are also very dependent on the type of machining, tool geometry, material to be machined, materials used for tool and coatings. Thus, this part is focused only on the description of the general wear mechanisms needed for the understanding of the wear properties of $Ti_{1-x}Al_xN$ coatings rather than an exhaustive description of these mechanisms.

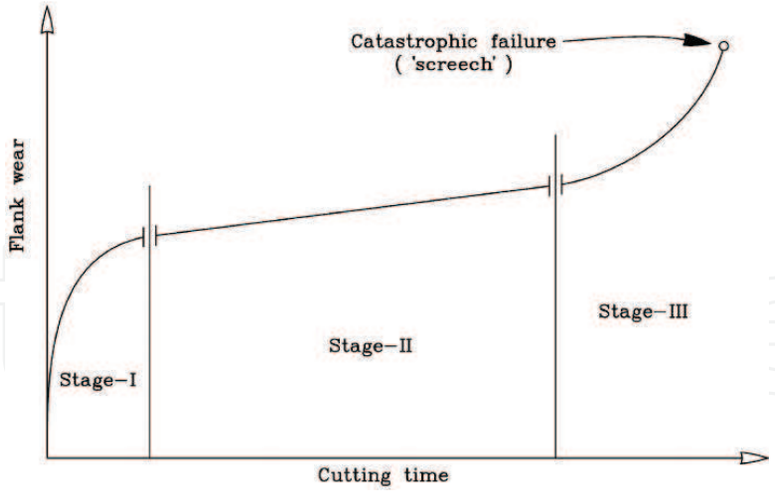

Figure 13. Three-step evolution of the flank wear of drills during drilling operations [97].

Wear can be divided into three steps, illustrated in **Figure 13** and showing the evolution of the flank wear of twist drills. Firstly, roughness can cause abrasive wear and the asperities are "removed" after welding to the cutting tool. This step is related to a high friction coefficient [64] associated with high wear rates [97]. The second step is characterized by both adhesive and abrasive wears. With increasing the cutting time, the continuous removal of workpiece particles by adhesive wear acts as a third-body, leading to abrasive wear. In this stage, the wear slowly increases linearly with time. The last stage is characterized by high wear rates leading to failure of the cutting tool [98]. The use of coatings as $Ti_{1-x}Al_xN$, because of their high hardness and diffusion barrier properties, allows to limit the abrasive and adhesive wears. The Al_2O_3 dense layer formed during cutting operations is also considered as the main factor responsible for the wear resistance of $Ti_{1-x}Al_xN$ coatings.

However, in addition to the wear mechanisms previously defined, coated tools are subjected to peening due to mechanical and thermal stresses, leading to the appearance of fatigue cracks that grow until coating failure [99]. Resistance to cracking of a coating can be estimated by the plastic deformation ratio, given by H^3/E^{*^2} with $E^* = E/(1-\nu^2)$, where H is the hardness, E^*, the effective Young modulus, E, the young modulus, and ν, the Poisson ratio of the coating. Better resistance to cracking could be obtained for the highest H^3/E^{*^2} values [78, 87, 100, 101]. Further details on wear mechanisms are given in [99, 102–105].

4.3.2. Coefficient of friction (COF)

The friction coefficient plays a key role in the first step of wear mechanisms, where a high wear rate is observed. However, the friction coefficient is dependent of many parameters such as the nature of the workpiece material, loading force, or growth direction of the coating [106, 107]. For these reasons, results available in literature show a high dispersion. Then, values of 1.4 were found for arc-deposited TiN sliding against M2 steel [108]. High values of about 1 were also obtained for CVD TiN coatings sliding against Al_2O_3. However, lower values of 0.3 to 0.45 were found for unbalance magnetron sputtering TiN against M42 steel [91]. These

lower values are reported to be due to the very thin oxide layer of several nanometers resulting from the elevation of the temperature at the contact interface between tool and workpiece.

Regarding the work of Shum et al. [91], addition of a small amount of aluminum in TiN leads to a huge increase of the COF (up to $x \approx 0.6$). A further increase of the aluminum content does not seem to strongly affect the COF, which stabilizes around 0.5 for $x = 0.6$. These results are confirmed for high aluminum contents in PACVD films [28]. In this study, both monophased films ($x = 0.79$) and biphased coatings ($x = 0.96$) have a COF around 0.5.

The temperature dependence of the COF does not seem to be clearly defined. Ohnuma et al. thus studied friction of $Ti_{0.6}Al_{0.4}N$, $Ti_{0.42}Al_{0.58}N$, and $Ti_{0.3}Al_{0.7}N$ coatings with fcc, fcc + hcp, and hcp structures, respectively, against AISI 304 material [109]. Measurements were performed at temperatures between 300 and 873 K. All coatings showed a COF between 0.6 and 0.9. Although a minimum value of 0.6 was found at 473 K for all coatings, no clear correlation between COF and temperature was found and the evolution of the COF vs. temperature could not be explained.

4.3.3. Wear properties of $Ti_{1-x}Al_xN$ coatings

Wear behavior is generally determined by studying the wear track obtained by pin-on-disc method [109] or multipass scratch test [91]. The results are highly dependent on many factors such as material characteristics (substrate, counterbody), deposition parameters, and testing parameters (critical loading force). It is thus difficult to make an exhaustive state of the art of the wear behavior. However, some overall results or trends can be identified.

Tests at room temperature seem to be highly related to the structure of the coatings. Studies show generally an increase of the wear resistance with increasing aluminum content in the fcc-$Ti_{1-x}Al_xN$ single-phased coatings, while the coatings with an fcc/hcp biphased structure, or only with the hcp structure, have a lower wear resistance [26, 64, 109, 110]. These results are consistent with the evolution of the hardness as a function of the aluminum content in the $Ti_{1-x}Al_xN$ coatings, influencing strongly the abrasive wear resistance of the coating. Tests performed at high temperatures show that $Ti_{1-x}Al_xN$ coatings have a better wear resistance than that of TiN. Ohnuma found thus a diminution of the wear track depth for temperatures above 600°C for $Ti_{1-x}Al_xN$ coatings whatever the structure, as shown in **Figure 14**. This behavior was related to the formation of the Al_2O_3 oxide layer, known to prevent adhesive wear [109]. Regarding the plasticity index H^3/E^{*2}, measurements show generally values above 0.1 [87] for $Ti_{1-x}Al_xN$ coatings, allowing to have better erosion resistance than other common nitrides such as TiN, CrN, or CrAlN [101].

4.3.4. In-service behavior of $Ti_{1-x}Al_xN$ coatings

Even though the previously defined wear tests allow to estimate the wear behavior of $Ti_{1-x}Al_xN$ coatings, machining tests are generally performed to determine accurately the in-service behavior of the coatings. The combined effects of several factors as stress and temperature, as well as tool geometry, can act strongly on the wear behavior of the coated tool. In the case of $Ti_{1-x}Al_xN$ coatings, only few literature is available on the influence of aluminum

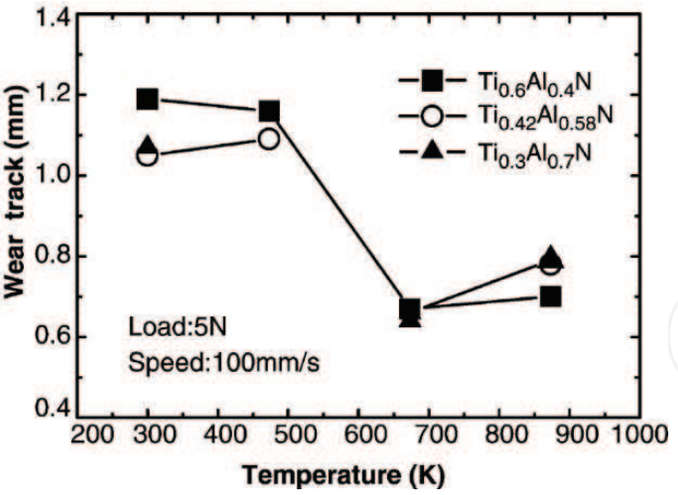

Figure 14. Evolution of wear track depth vs. temperature for coatings with different crystallographic structures (single-phase cubic for x = 0.4, two-phase cubic/hexagonal for 0.58, and single-phase hexagonal for x = 0.7) [109].

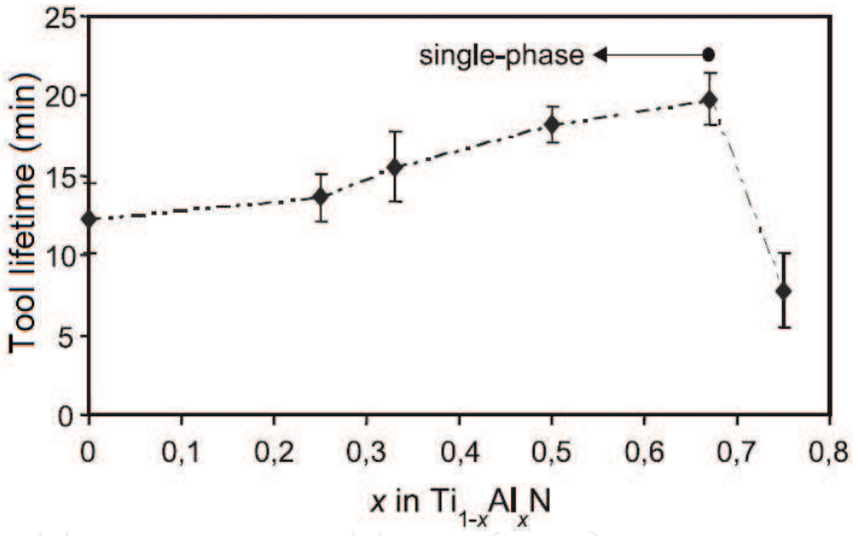

Figure 15. Evolution of the tool lifetime vs. Al content for $Ti_{1-x}Al_xN$ coatings [26].

content in $Ti_{1-x}Al_xN$ during machining tests like milling or drilling. However, it appears that even small amounts of aluminum in TiN coatings lead to a strong increase of the tool lifetime [50, 64, 111]. Hörling et al. also showed that increasing aluminum content in the cubic $Ti_{1-x}Al_xN$ single-phased coatings led to a continuous increase of the tool lifetime until $x \approx 0.66$ (**Figure 15**). This behavior should be related to the higher hardness as well as a better oxidation resistance [26, 110]. A further increase of the aluminum content leads to a drop of the tool lifetime due to the presence of hcp-AlN with poor mechanical properties.

More details about the influence of machining parameters (cutting speed, cutting tool material, and geometry) on the wear and breakage mechanisms of $Ti_{1-x}Al_xN$-coated tools during

machining of high-speed steel, Ni-based superalloys, aluminum and titanium alloys are reported in [99, 112–114], respectively.

5. Summary

In this chapter, the thermodynamical basis, deposition, and some mechanical and chemical properties of coatings based on $Ti_{1-x}Al_xN$ and $Ti_{1-x}Al_xSi_yN$ have been reviewed. The general mechanisms (hardening effect, oxidation mechanisms, and wear mechanisms) associated to these properties were also discussed by pointing out the influence of the temperature and the aluminum content in the films. Increasing aluminum content induces structural changes that are directly associated with the properties. The high thermal stability and the age-hardening effect, observed in titanium-aluminum nitride-based coatings, are related to the coherent spinodal decomposition in the Ti-Al-N system. Concerning elaboration by means of CVD based processes, the stabilization of the fcc-$Ti_{1-x}Al_xN$ metastable solid solution can be achieved by a combination of relatively low deposition temperatures, high partial pressures of reactive precursors, and low total pressure. As-deposited monolayer coatings show a higher hardness and a better oxidation resistance when aluminum content is increased. Hardness up to about 30 GPa and stability in air up to 800°C have been measured. These values outperform the typical values of about 25 GPa for hardness and 500°C for the temperature of starting oxidation found for usual TiN coatings. These properties are related to the B1-structure observed for $Ti_{1-x}Al_xN$ coatings with x up to 0.7 for PVD and 0.9 for PACVD and CVD processes. In in-service conditions, an increase of hardness and oxidation resistance is also observed. The increased hardness is related to the so-called age-hardening effect observed at elevated temperature (≈800°C) in the Ti-Al-N system and the enhancement of oxidation resistance is associated to the formation of a dense and protective Al_2O_3 top-layer. The adjustment of the aluminum content and the control of the cutting parameters lead to better wear resistance and tool lifetime in machining operations, for which both high mechanical and chemical stabilities are required.

Acknowledgements

The authors would like to acknowledge the CEA Saclay, Direction du Programme Matériaux Avancés and Groupement d'Intérêt Public Haute-Marne (GIP 52) for their financial support.

A. Appendix

Summary of mechanical properties depending on Aluminum content and structure of $Ti_{1-x}Al_xN$ $Ti_{1-x}Al_xN$ coatings obtained by different deposition processes.

Ref.	x	Structure	Process	Substrate	Deposition temperature (°C)	Pressure (Pa)	Bias voltage (V)	Discharge voltage (V)	Residual stresses (GPa)	Hardness (Gpa)	Young modulus (Gpa)
[23]	0	fcc	Magnetron sputtering	Si	500°C	0.40	−60	/	−1356	22.8	378
	0.62	fcc	Magnetron sputtering	Si	500°C	0.40	−60	/	−0.883	31.3	≈380
	0.67	fcc/hcp	Magnetron sputtering	Si	500°C	0.40	−60	/	+0.102	27.2	≈320
	0.75	hcp	Magnetron sputtering	Si	500°C	0.40	−60	/	+0.186	22.9	≈255
[26]	0	fcc	Arc evaporation	WC/Co-6%	500°C	/	/	/	−2.9	28.5	617
	0.66	fcc	Arc evaporation	WC/Co-6%	500°C	/	/	/	−3.1	32.6	627
	0.74	fcc/hcp	Arc evaporation	WC/Co-6%	500°C	/	/	/		32.3	595
[90]	≈0.5	fcc	Arc evaporation	WC/Co-6%		/	−40 to −200	/	−1.7 to −5		
[3]	0	fcc	Close-field magnetron	M42 steel or Si	Room temperature	0.27	−50	/	≈ − 3	23	245.3
	0.41	fcc	Close-field magnetron	M42 steel or Si	Room temperature	0.27	−50	/	≈ − 0.35	31.4	315.2
	0.48	fcc/hcp	Close-field magnetron	M42 steel or Si	Room temperature	0.27	−50	/	≈ − 0.45	28.5	304.8
	1	hcp	Close-field magnetron	M42 steel or Si	Room temperature	0.27	−50	/	≈ − 1.5	13.8	175.2
[19]	0.66	fcc	Cathodic arc evaporation	WC/Co		/	/	/	/	≈37.5	/
[115]	0.48	fcc	Cathodic arc evaporation	WC/Co	550°C	2.00	−100	/	/	31.2	/
[98]	0	fcc	Cathodic arc ion plating	WC/Co	450°C	2–5	−50	/	/	≈20	/
	0.6	fcc	Cathodic arc ion plating	WC/Co	450°C	2–5	−50	/	/	≈30	/

Ref.	x	Structure	Process	Substrate	Deposition temperature (°C)	Pressure (Pa)	Bias voltage (V)	Discharge voltage (V)	Residual stresses (GPa)	Hardness (Gpa)	Young modulus (Gpa)
	0.85	hcp	Cathodic arc ion plating	WC/Co	450°C	2–5	−50	/	/	≈18.6	/
[25]	0	fcc	Cathodic arc ion plating	(Mo)	400°C	0.40	−100	/	/	≈20.6	/
	0.6	fcc	Cathodic arc ion plating	(Mo)	400°C	0.40	−100	/	/	≈31.4	/
	0.7	fcc/hcp	Cathodic arc ion plating	(Mo)	400°C	0.40	−100	/	/	≈27	/
	0.85	hcp	Cathodic arc ion plating	(Mo)	400°C	0.40	−100	/	/	≈19.6	/
[110]	0	fcc	Reactive DC magnetron	SKH51	350°C	0.80	−80	/	/	≈23.5	/
	0.5	fcc	Reactive DC magnetron	SKH51	350°C	0.80	−80	/	/	≈37.2	/
	0.6	fcc/hcp	Reactive DC magnetron	SKH51	350°C	0.80	−80	/	/	≈21.6	/
[116]	0.5	fcc	Cathodic arc evaporation	WC/Co	450°C	3.20	−40	/	−2.48	27.1	515
[64]	0	fcc	PACVD	Z85 WCDV	500°C	50–100	/	150	+0.3	≈29	≈490
	0.64	fcc	PACVD	Z85 WCDV	500°C	50–100	/	300	−3.2	≈25.7	≈365
[28]	0.02	fcc	PACVD	H11 steel or WC/Co	510°C	150	/	430	/	≈23.5	/
	0.83	fcc	PACVD	H11 steel or WC/Co	510°C	150	/	480	/	38.7	/
	0.91	fcc/hcp	PACVD	H11 steel or WC/Co	510°C	150	/	530	/	≈49	/
[27]	0.82	fcc	LPCVD	WC/6%Co-TiN	800°C	<10.000	/	/	/	29.2	444
	0.9	fcc	LPCVD		800°C	<10.000	/	/	/	32.4	539

http://dx.doi.org/10.5772/intechopen.79747

Ref.	x	Structure	Process	Substrate	Deposition temperature (°C)	Pressure (Pa)	Bias voltage (V)	Discharge voltage (V)	Residual stresses (GPa)	Hardness (Gpa)	Young modulus (Gpa)
				WC/6%Co-TiN							
	0.82	fcc	LPCVD	WC/6%Co-TiN	850°C	<10.000	/	/	−0.45	/	/
	0.82	fcc	LPCVD	WC/6%Co-TiN	800°C	<10.000	/	/	−0.92	/	/

http://dx.doi.org/10.5772/intechopen.79747

Author details

Florent Uny[1,2]*, Elisabeth Blanquet[3], Frédéric Schuster[4] and Frédéric Sanchette[1,2]

*Address all correspondence to: florent.uny@utt.fr

1 ICD-LASMIS, Université de Technologie de Troyes, CNRS, Antenne de Nogent, Pôle Technologique de Haute-Champagne, Nogent, France

2 Nogent International Center for CVD Innovation, LRC CEA-ICD-LASMIS, UTT, Antenne de Nogent, Pôle Technologique de Haute-Champagne, Nogent, France

3 Université Grenoble Alpes, CNRS, Grenoble INP, SIMaP, Grenoble, France

4 Centre CEA de Saclay, France

References

[1] Damond E, Revêtements PVD. Durs Pour la mécanique. Développement d'un réacteur PVD Industriel et de Deux revêtements Multicouches associés. Mém. DPE En Génie Procédés; 2000

[2] Jin N, Yang Y, Luo X, Xia Z. Development of CVD Ti-containing films. Progress in Materials Science. 2013;**58**(8):1490-1533

[3] Shum P, Li K, Zhou Z, Shen Y. Structural and mechanical properties of titanium-aluminium-nitride films deposited by reactive close-field unbalanced magnetron sputtering. Surface and Coating Technology. 2004;**185**(2-3):245-253

[4] Veprek S, Veprek-Heijman MGJ, Karvankova P, Prochazka J. Different approaches to superhard coatings and nanocomposites. Thin Solid Films. 2005;**476**(1):1-29

[5] Rachbauer R, Gengler JJ, Voevodin AA, Resch K, Mayrhofer PH. Temperature driven evolution of thermal, electrical, and optical properties of Ti-Al-N coatings. Acta Materialia. 2012;**60**(5):2091-2096

[6] Rebouta L et al. Optical characterization of TiAlN/TiAlON/SiO_2 absorber for solar selective applications. Surface and Coating Technology. 2012;**211**:41-44

[7] Man BY, Guzman L, Miotello A, Adami M. Microstructure, oxidation and H2-permeation resistance of TiAlN films deposited by DC magnetron sputtering technique. Surface and Coating Technology. 2004;**180-181**:9-14

[8] Zhou M, Makino Y, Nose M, Nogi K. Phase transition and properties of Ti-Al-N thin films prepared by RF plasma assisted magnetron sputtering. Thin Solid Films. 1999;**339**:203-208

[9] Bartosik M et al. Thermal expansion of Ti-Al-N and Cr-Al-N coatings. Scripta Materialia. 2017;**127**:182-185

[10] Favvas EP, Mitropoulos AC. What is spinodal decomposition? Journal of Engineering Science and Technology Review. 2008;**1**:25-27

[11] Schuster JC, Bauer J. The ternary system titanium-aluminum-nitrogen. Journal of Solid State Chemistry. 1984;**53**(2):260-265

[12] Cabioch T, Alkazaz M, Beaufort M-F, Nicolai J, Eyidi D, Eklund P. Ti_2AlN thin films synthesized by annealing of (Ti+Al)/AlN multilayers. Materials Research Bulletin. 2016; **80**:58-63

[13] Han YS, Kalmykov KB, Dunaev SF, Zaitsev AI. Phase equilibria in the Ti-Al-N system at 1273 K. Doklady Physical Chemistry. 2004;**396**:134-137

[14] Holleck H. Metastable coatings—Prediction of composition and structure. Surface and Coating Technology. 1988;**36**(1-2):151-159

[15] Chen Q, Sundman B. Thermodynamic assessment of the Ti-Al-N system. Journal of Phase Equilibria. 1988;**19**(2):146-160

[16] Tomashik V, Perrot P. Aluminium-Nitrogen-Titanium. Springer London. Landolt-Bornstein. 2005;**11A3**:322-332

[17] Stolten H. Doctoral Thesis, RTWH Aachen; 1991

[18] Saunders N, Miodownik AP. The use of free energy vs composition curves i the deposition of phase formation in codeposited alloy thin films. Calphad. 1985;**9**(3):283-290

[19] Mayrhofer PH et al. Self-organized nanostructures in the Ti-Al-N system. Applied Physics Letters. 2003;**83**(10):2049

[20] Anderbouhr S, Gilles S, Blanquet E, Bernard C, Madar R. Thermodynamic modeling of the Ti-Al-N system and application to the simulation of CVD processes of the (Ti, Al)N metastable phase. Chemical Vapor Deposition. 1999;**5**(3):109-115

[21] Gilles S, Bourhila N, Ikeda S, Bernard C, Madar R. Deposition of TiAlN thin films by MOCVD - thermodynamic predictions and experimental results. Surface and Coating Technology. 1997;**94-95**:285-290

[22] Stolten H, Spencer P, Neuschütz D. Estimation of formation enthalpies for transition metal mono nitrides, carbides, oxides. Journal de Chimie Physique. 1993;**90**:209-219

[23] Chen L, Paulitsch J, Du Y, Mayrhofer PH. Thermal stability and oxidation resistance of Ti-Al-N coatings. Surface and Coating Technology. 2012;**206**(11-12):2954-2960

[24] Vaz F, Rebouta L, Andritscky M, da Silva MF, Soares JC. Thermal oxidation of TiAlN coatings in air. Journal of the European Ceramic Society. 1997;**17**:1971-1977

[25] Ikeda T, Satoh H. Phase formation and characterization of hard caotings in the Ti-Al-N system prepared by cathodic arc ion plating. Thin Solid Films. 1991;**195**:99-110

[26] Hörling A, Hultman L, Odén M, Sjölén J, Karlsson L. Mechanical properties and machining performance of $Ti_{1-x}Al_xN$-coated cutting tools. Surface and Coating Technology. 2005;**191**(2-3):384-392

[27] Endler I et al. Novel aluminum-rich $Ti_{1-x}Al_xN$ coatings by LPCVD. Surface and Coating Technology. 2008;**203**(5-7):530-533

[28] Prange R, Cremer R, Neuschütz D. PECVD of TiAlN films from chlridric precursors in a DC glow discharge. Surface and Coating Technology. 2000;**133-134**:208-214

[29] Jarms C, Stock H-R, Mayr P. Mechanical properties, structure and oxidation behaviour of $Ti_{1-x}Al_xN$-hard coatings deposited by pulsed dc plasma-assisted chemical vapour deposition (PACVD). Surface and Coating Technology. 1998;**108**:206-210

[30] Cremer R, Arndt M, Neuschütz D. Experimental determination of the metastable (Ti, Al) N diagram up to 700°C. Value-Addition Metallurgy. 1998:249-258

[31] Spencer PJ. Computational thermochemistry - from its early caphad days to a cost effective role in materials development and processing. Calphad. 2001;**25**(2):163-174

[32] Mayrhofer PH, Music D, Schneider JM. Ab initio calculated binodal and spinodal of cubic $Ti_{1-x}Al_xN$. Applied Physics Letters. 2006;**88**(7):071922

[33] Shulumba N, et al. Anharmonicity changes the solid solubility of a random alloy at high temperatures, ArXiv Prepr. 2015. ArXiv150302459

[34] Zhang RF, Veprek S. Metastable phases and spinodal decomposition in $Ti_{1-x}Al_xN$ system studied by ab initio and thermodynamic modeling, a comparison with the TiN-Si_3N_4 system. Materials Science and Engineering A. 2007;**448**(1-2):111-119

[35] Cahn JW. On spinodal decomposition. Acta Metallurgica. 1961;**9**:795-801

[36] Cahn JW, Hilliard JE. Spinodal decomposition - a reprise. Acta Metallurgica. 1971;**19**: 151-161

[37] Zhou J et al. Phase equilibria, thermodynamics and microstructure simulation of metastable spinodal decomposition in c–$Ti_{1-x}Al_xN$ coatings. Calphad. 2017;**56**:92-101

[38] Alling B, Odén M, Hultman L, Abrikosov IA. Pressure enhancement of the isostructural cubic decomposition in $Ti_{1-x}Al_xN$. Applied Physics Letters. 2009;**95**(18):181906

[39] Yang B et al. Thermal and thermo-mechanical properties of Ti-Al-N and Cr-Al-N coatings. International Journal of Refractory Metals and Hard Materials. 2012;**35**:235-240

[40] Chen L, Yang B, Xu Y, Pei F, Zhou L, Du Y. Improved thermal stability and oxidation resistance of Al-Ti-N coating by Si addition. Thin Solid Films. 2014;**556**:369-375

[41] Xu YX, Chen L, Pei F, Du Y, Liu Y, Yue JL. Influence of Hf on the structure, thermal stability and oxidation resistance of Ti-Al-N coatings. Thin Solid Films. 2014;**565**:25-31

[42] Rachbauer R, Holec D, Mayrhofer PH. Increased thermal stability of Ti-Al-N thin films by ta alloying. Surface and Coating Technology. 2012;**211**:98-103

[43] Wagner J, Edlmayr V, Penoy M, Michotte C, Mitterer C, Kathrein M. Deposition of Ti-Al-N coatings by thermal CVD. International Journal of Refractory Metals and Hard Materials. 2008;**26**(6):563-568

[44] Keckes J et al. Self-organized periodic soft-hard nanolamellae in polycrystalline TiAlN thin films. Thin Solid Films. 2013;**545**:29-32

[45] Todt J et al. Superior oxidation resistance, mechanical properties and residual stresses of an Al-rich nanolamellar $Ti_{0.05}Al_{0.95}N$ coating prepared by CVD. Surface and Coating Technology. 2014;**258**:1119-1127

[46] Kyrylov O, Cremer R, Neuschütz D, Prange R. Correlation between plasma conditions and properties of (Ti, Al) N coatings deposited by PECVD. Surface and Coating Technology. 2002;**151**:359-364

[47] Todt J et al. Al-rich cubic $Al_{0.8}Ti_{0.2}N$ coating with self-organized nano-lamellar microstructure: Thermal and mechanical properties. Surface and Coating Technology. 2016; **291**:89-93

[48] Zalesak J et al. Peculiarity of self-assembled cubic nanolamellae in the TiN/AlN system: Epitaxial self-stabilization by element deficiency/excess. Acta Materialia. 2017;**131**:391-399

[49] Zalesak J et al. Combinatorial refinement of thin-film microstructure, properties and process conditions: Iterative nanoscale search for self-assembled TiAlN nanolamellae. Journal of Applied Crystallography. 2016;**49**(6):2217-2225

[50] Sanchette F, Ducros C, Schmitt T, Steyer P, Billard A. Nanostructured hard coatings deposited by cathodic arc deposition: From concepts to applications. Surface and Coating Technology. 2011;**205**(23-24):5444-5453

[51] Sanders DM. Review of ion-based coating processes derived from the cathodic arc. Journal of Vacuum Science & Technology A: Vacuum, Surfaces, and Films. 1989;**7**(3):2339

[52] Sanders DM, Boercker DB, Falabella S. Coating technology based on the vacuum arc-a review. IEEE Transactions on Plasma Science. 1990;**18**(6):883-894

[53] Anders A, Anders S, Jüttner B, Pursch H, Bötticher W, Lück H. Vacuum arc cathode spot parameters from high-resolution luminosity measurements. Journal of Applied Physics. 1992;**71**(10):4763-4770

[54] Ducros C, Cayron C, Sanchette F. Multilayered and nanolayered hard nitride thin films deposited by cathodic arc evaporation. Part 1: Deposition, morphology and microstructure. Surface and Coating Technology. 2006;**201**(1-2):136-142

[55] Ducros C, Sanchette F. Multilayered and nanolayered hard nitride thin films deposited by cathodic arc evaporation. Part 2: Mechanical properties and cutting performances. Surface and Coating Technology. 2006;**201**(3-4):1045-1052

[56] Kafizas A, Carmalt CJ, Parkin IP. CVD and precursor chemistry of transition metal nitrides. Coordination Chemistry Reviews. 2013;**257**(13-14):2073-2119

[57] Sun YM, Endle JP, Ekerdt JG, Russell NM, Healy MD, White JM. Aluminum titanium nitride films grown with multpile precursors. Materials Science in Semiconductor. Processing. 1999;**2**:253-261

[58] Endle JP, Sun YM, Nguyen N, Cowley AH, White JM, Ekerdt JG. Titanium-aluminum nitride film growth and related chemistry using dimethylamino-based precursors. Thin Solid Films. 2001;**385**:66-73

[59] Xu Y, Yan X-T. Chemical Vapour Deposition. London: Springer London; 2010

[60] Pons M, Bernard C, Madar R. Numerical modelling for CVD simulation and process optimization: Coupled thermochemical and mass transport approaches. Surface and Coating Technology. 1993;**61**(1-3):274-281

[61] Kleijn CR. Computational modeling of transport phenomena and detailed chemistry in chemical vapor deposition-a benchmark solution. Thin Solid Films. 2000;**365**(2):294-306

[62] Bernard C, Pons M. Vapor transport processing: Models and simulations. In: Reference Module in Materials Science and Materials Engineering. New York; Elsevier: 2016

[63] Choy KL. Chemical vapour deposition of coatings. Progress in Materials Science. 2003;**48** (2):57-170

[64] Anderbouhr S. Depot Chimique en Phase Vapeur de Couches Minces de (Ti,Al)N à Composition Variable, [Doctoral Thesis]. Institu National Polytechnique de Grenoble; 1999

[65] Anderbouhr S et al. LPCVD and PACVD (Ti, Al) N films: Morphology and mechanical properties. Surface and Coating Technology. 1999;**115**(2):103-110

[66] Cross JB, Schlegel HB. Molecular orbital studies of titanium nitride chemical vapor deposition: Gas phase complex formation, ligand exchange, and elimination reactions. Chemistry of Materials. 2000;**12**(8):2466-2474

[67] Jeo D, Hwang J, Chae H. Temperature dependence of $TiCl_4$ and NH_3 surface reactions in CVD trap systems. Journal of the Korean Physical Society. 2009;**54**(3):1087-1090

[68] Bryant WA. The fundamentals of chemical vapour deposition. Journal of Materials Science. 1977;**12**(7):1285-1306

[69] Van der Drift A. Evolutionary selection, a principle governing growth orientation in vapor-deposited layers. Philips Research Reports. 1967;**22**:267-288

[70] Cheng H-E, Wen Y-W. Correlation between process parameters, microstructure and hardness of titanium nitride films by chemical vapor deposition. Surface and Coating Technology. 2004;**179**(1):103-109

[71] Cheng HE, Hon MH. Texture formation in titanium nitride films prepared by chemical vapor deposition. Journal of Applied Physics. 1996;**79**(10):8047

[72] Wagner J, Mitterer C, Penoy M, Michotte C, Wallgram W, Kathrein M. The effect of deposition temperature on microstructure and properties of thermal CVD TiN coatings. International Journal of Refractory Metals and Hard Materials. 2008;**26** (2):120-126

[73] Cheng H-E, Hon M-H. Growth mechanism of star-shaped TiN crystals. Journal of Crystal Growth. 1994;**142**(1):117-123

[74] Tang S, Wang J, Zhu Q, Chen Y, Li X. Oxidation behavior of CVD star-shaped TiN coating in ambient air. Ceramics International. 2015;**41**(8):9549-9554

[75] HAkansson G, Hultla L, Sundgren JE, Greene JE, Münz WD. Microstructures of TiN films grown by various physical vapour deposition. Surface and Coating Technology. 1991;**48**:51-67

[76] Rebenne HE, Bhat DG. Review of CVD TiN coatings for wear-resistant applications: Deposition processes, properties and performance. Surface and Coating Technology. 1994;**63**(1-2):1-13

[77] Park IW, Kim KH. Coating materials of TiN, TiAlN, TiSiN by PECVD for mechanical applications. Journal of Materials Processing Technology. 2002;**130-11**:254-259

[78] Pemmasani SP et al. Effect of microstructure and phase constitution on mechanical properties of $Ti_{1-x}Al_xN$ coatings. Applied Surface Science. 2014;**313**:936-946

[79] Grossmann B, Schalk N, Czettl C, Pohler M, Miterrer C. Phase composition and thermal stability of arc evaporated $Ti_{1-x}Al_xN$. Surface and Coating Technology. 2017;**309**:687-693

[80] Shimizu T, Komiya H, Teranishi Y, Morikawa K, Nagasaka H, Yang M. Pressure dependence of (Ti, Al)N film growth on inner walls of small holes in high-power impulse magnetron sputtering. Thin Solid Films. 2017;**624**:189-196

[81] IHI Ion Bond AG. Personal Communication

[82] Mayrhofer PH, Music D, Schneider JM. Influence of the Al distribution on the structure, elastic properties, and phase stability of supersaturated $Ti_{1-x}Al_xN$. Journal of Applied Physics. 2006;**100**(9):094906

[83] Shieh J, Hon MH. Nanostructure and hardness of TiAlN prepared by PECVD. Thin Solid Films. 2001;**391**:101-108

[84] Musil J, Hruby H. Superhard nanocomposite TiAlN films prepared by magnetron sputtering. Thin Solid Films. 2000;**365**:104-109

[85] Quinto DT, Wolfe GJ, Jindal PC. High temperature microhardness of hard coatings produced by PVD and CVD. Thin Solid Films. 1987;**153**:19-36

[86] Hakansson G, Sundgren JE, McIntyre D, Greene JE, Münz WD. Microstructure and physical properties of polycrystalline metastable $Ti_{0.5}Al_{0.5}N$ grown by DC magnetron sputtering. Thin Solid Films. 1987;**153**:55-65

[87] Elmkhah H, Zhang TF, Abdollah-zadeh A, Kim KH, Mahboubi F. Surface characteristics for the TiAlN coatings deposited by high power impulse magnetron sputtering technique at the different bias voltages. Journal of Alloys and Compounds. 2016;**688**: 820-827

[88] Hoffman RW. Stresses in thin films: The relevance of grain boundaries and impurities. Thin Solid Films. 1976;**34**(2):185-190

[89] Cheng G, Han D, Liang C, Wu X, Zheng R. Influence of residual stress on mechanical properties of TiAlN thin films. Surface and Coating Technology. 2013;**228**:S328-S330

[90] Ahlgren M, Blomqvist H. Influence of bias variation on residual stress and texture in TiAlN PVD coatings. Surface and Coating Technology. 2005;**200**(1-4):157-160

[91] Shum PW, Tam WC, Li KY, Zhou ZF, Shen YG. Mechanical and tribological properties of titanium-aluminium-nitride films deposited by reactive close-field unbalanced magnetron sputtering. Wear. 2004;**257**(9-10):1030-1040

[92] Kitagawa T, Kubo A, Maekawa K. Temperature and wear of cutting tools in high-speed machining of Inconel 718 and Ti-6Al-V-2Sn. Wear. 1997;**202**:142-148

[93] Joshi A, Hu HS. Oxidation behavior of titanium-aluminium nitrides. Surface and Coating Technology. 1995;**76-77**:499-507

[94] mc Intyre D, Greene JE, hakansson G, Sundgren JE, Münz WD. Oxidation of metastable single-phase polycrystlline $Ti_{0.5}Al_{0.5}N$ films - kinetics and mechanisms. Journal of Applied Physics. 1990;**67**:1542

[95] Hugon MC, Desvignes JM, Agius B, Vickridge IC, Kim DJ, Kingon AI. Narrow resonance profiling study of the oxidation of reactively sputtered TiAlN thin films. Nuclear Instruments and Methods in Physics Research B. 2000;**161-163**:578-583

[96] Kim CW, Kim KH. Anti-oxidation of TiAlN film prepared by plasma-assisted chemicalm vapor deposition and roles of Al. Thin Solid Films. 1997;**307**:113-119

[97] Harris S, Doyle E, Vlasveld A, Audy J, Quick D. A study of the wear mechanisms of $Ti_{1-x}Al_xN$ and $Ti_{1-x-y}Al_xCr_yN$ coated high-speed steel twist drills under dry machining conditions. Wear. 2003;**254**(7-8):723-734

[98] Burant RO, McGinty MJ, Friedrich MO. Cutting tools/drills-fundamentals. Manufacturing Engineering. 1979;**83**:29-31

[99] Wang CY, Xie YX, Qin Z, Lin HS, Yuan YH, Wang QM. Wear and breakage of TiAlN- and TiSiN-coated carbide tools during high-speed milling of hardened steel. Wear. 2015;**336-337**:29-42

[100] Feng C et al. Effects of Si content on microstructure and mechanical properties of TiAlN/Si_3N_4-Cu nanocomposite coatings. Applied Surface Science. 2014;**320**:689-698

[101] Deng J, Wu F, Lian Y, Xing Y, Li S. Erosion wear of CrN, TiN, CrAlN, and TiAlN PVD nitride coatings. International Journal of Refractory Metals and Hard Materials. 2012;**35**: 10-16

[102] Dolinšek S, Šuštaršič B, Kopač J. Wear mechanisms of cutting tools in high-speed cutting processes. Wear. 2001;**250**(1):349-356

[103] Holmberg K, Matthews A, Ronkainen H. Coatings tribology—Contact mechanisms and surface design. Tribology International. 1998;**31**(1):107-120

[104] Kagnaya MT. Contribution à l'identification Des mécanismes d'usure d'un WC-Co en Usinage et Par Approche Tribologique et Thermique. Ecole Nationale Supérieure des Mines de Paris; 2009

[105] Santecchia E, Hamouda AMS, Musharavati F, Zalnezhad E, Cabibbo M, Spigarelli S. Wear resistance investigation of titanium nitride-based coatings. Ceramics International. 2015;**41**(9):10349-10379

[106] Ma G, Wang L, Gao H, Zhang J, Reddyhoff T. The friction coefficient evolution of a TiN coated contact during sliding wear. Applied Surface Science. 2015;**345**:109-115

[107] Azushima A, Tanno Y, Iwata H, Aoki K. Coefficients of friction of TiN coatings with preferred grain orientations under dry condition. Wear. 2008;**265**(7-8):1017-1022

[108] Wilson S, Alpas AT. TiN coating wear mechanisms in dry sliding contact against high speed steel. Surface and Coating Technology. 1998;**108**:369-376

[109] Ohnuma H, Nihira N, Mitsuo A, Toyoda K, Kubota K, Aizawa T. Effect of aluminum concentration on friction and wear properties of titanium aluminum nitride films. Surface and Coating Technology. 2004;**177-178**:623-626

[110] Lii D-F. The effects of aluminium composition on the mechanical properties of reactivity sputtered TiAlN films. Journal of Materials Science. 1998;**33**(8):2137-2145

[111] Tanaka Y. Properties of (Ti1-xAlx)N coatings for cutting tools prepared by the cathodic arc ion plating method. Journal of Vacuum Science & Technology A: Vacuum, Surfaces, and Films. 1992;**10**(4):1749

[112] Bhatt A, Attia H, Vargas R, Thomson V. Wear mechanisms of WC coated and uncoated tools in finish turning of Inconel 718. Tribology International. 2010;**43**(5–6):1113-1121

[113] Nouari M, List G, Girot F, Géhin D. Effect of machining parameters and coating on wear mechanisms in dry drilling of aluminium alloys. International Journal of Machine Tools and Manufacture. 2005;**45**(12-13):1436-1442

[114] Arulkirubakaran D, Senthilkumar V. Performance of TiN and TiAlN coated micro-grooved tools during machining of Ti-6Al-4V alloy, Int. Journal of Refractory Metals and Hard Materials. 2017;**62**:47-57

[115] Wang SQ et al. Effect of Si addition on microstructure and mechanical properties of Ti-Al-N coating. International Journal of Refractory Metals and Hard Materials. 2010;**28**(5): 593-596

[116] Zhu L, Song C, Ni W, Liu Y. Effect of 10% Si addition on cathodic arc evaporated TiAlSiN coatings. Transactions of Nonferrous Metals Society of China. 2016;**26**(6):1638-1646